Electronic Supplementary Material (ESI) for Environmental Science: Nano.

Supporting information

Effect of NOM on copper sulfide nanoparticle growth, stability, and oxidative dissolution

Kevin Hoffmann,[a] Sylvain Bouchet,[a] Iso Christl,[a] Ralf Kaegi,[b] and Ruben Kretzschmar[a,*]

[a] ETH Zürich, Institute of Biogeochemistry and Pollutant Dynamics, CHN, 8092 Zürich, Switzerland

[b] Eawag, Swiss Federal Institute of Aquatic Science and Technology, 8060 Dübendorf, Switzerland

*Corresponding author: ruben.kretzschmar@env.ethz.ch

41 pages, 22 figures, 10 tables

Figures

Tables

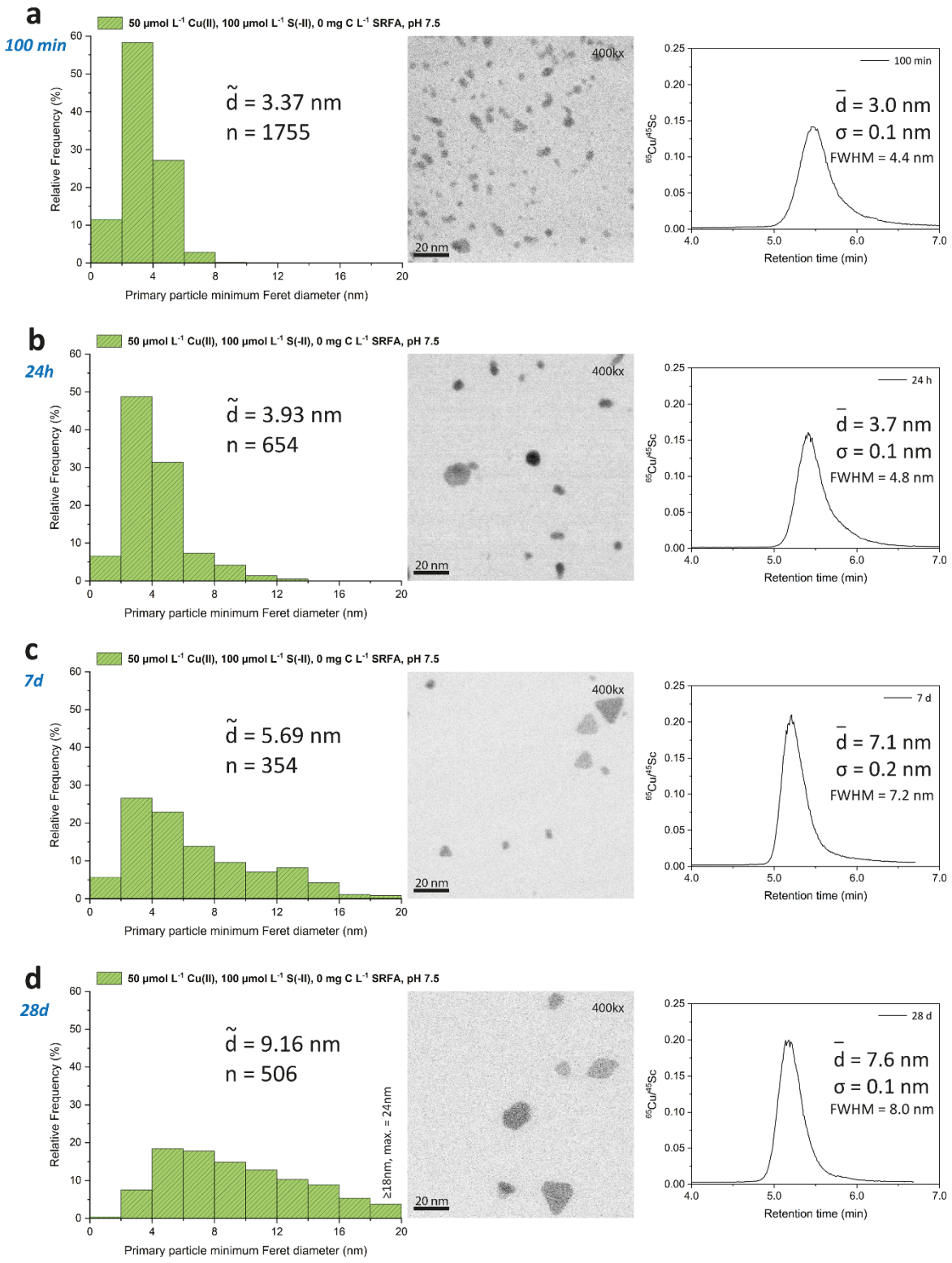

Figure S1: Particle size distributions (PSD) of Cu_xS particles (left panels) from dilute (50 µmol L^{-1} Cu(II), 100 µmol L^{-1} S(-II)) suspensions (at pH 7.5 and an ionic strength of 10 mmol L^{-1} NaCl) derived from TEM images (middle panels) absent in SRFA (0 mg C L^{-1}) after 100 min (a), 24 h (b), 7 d (c) and 28 d (d) with median TEM diameters ($\tilde{d}$) and number of counted particles (n). Counted particles larger than the given PSD limits were binned within the largest shown size bin, with size of the largest particle indicated (max.). HAADF-TEM images (shown as inverted images in the middle panels) show Cu_xS nanoparticles from corresponding suspensions. Size exclusion chromatograms of these suspensions (internal standard corrected ^{65}Cu signal displayed as intensity values) show retention time shifts in the course of the growth experiment with converted average SEC diameters ($\bar{d}$), standard deviation (σ) of triplicate samples (n=3) and full width at half maximum (FWHM).

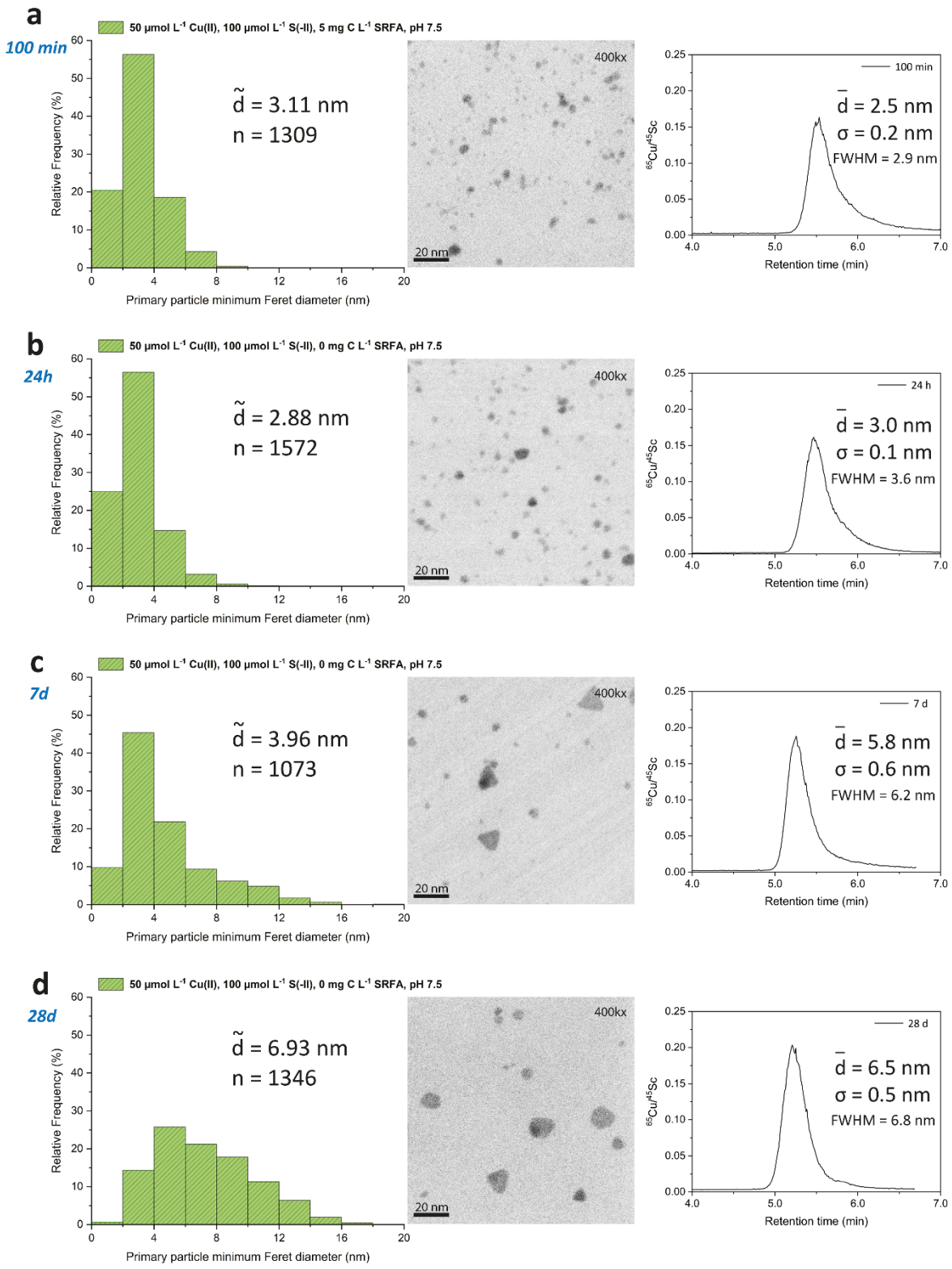

Figure S2: Particle size distributions (PSD) of Cu_xS particles (left panels) from dilute (50 µmol L^{-1} Cu(II), 100 µmol L^{-1} S(-II)) suspensions (at pH 7.5 and an ionic strength of 10 mmol L^{-1} NaCl) derived from TEM images (middle panels) in the presence of 5 mg C L^{-1} SRFA after 100 min (a), 24 h (b), 7 d (c) and 28 d (d) with median TEM diameters ($\tilde{d}$) and number of counted particles (n). HAADF-TEM images (shown as inverted images in the middle panels) show Cu_xS nanoparticles from corresponding suspensions. Size exclusion chromatograms of these suspensions (internal standard corrected ^{65}Cu signal displayed as intensity values) show retention time shifts in the course of the growth experiment with converted average SEC diameters ($\bar{d}$),standard deviation (σ) of triplicate samples (n=3) and full width at half maximum (FWHM).

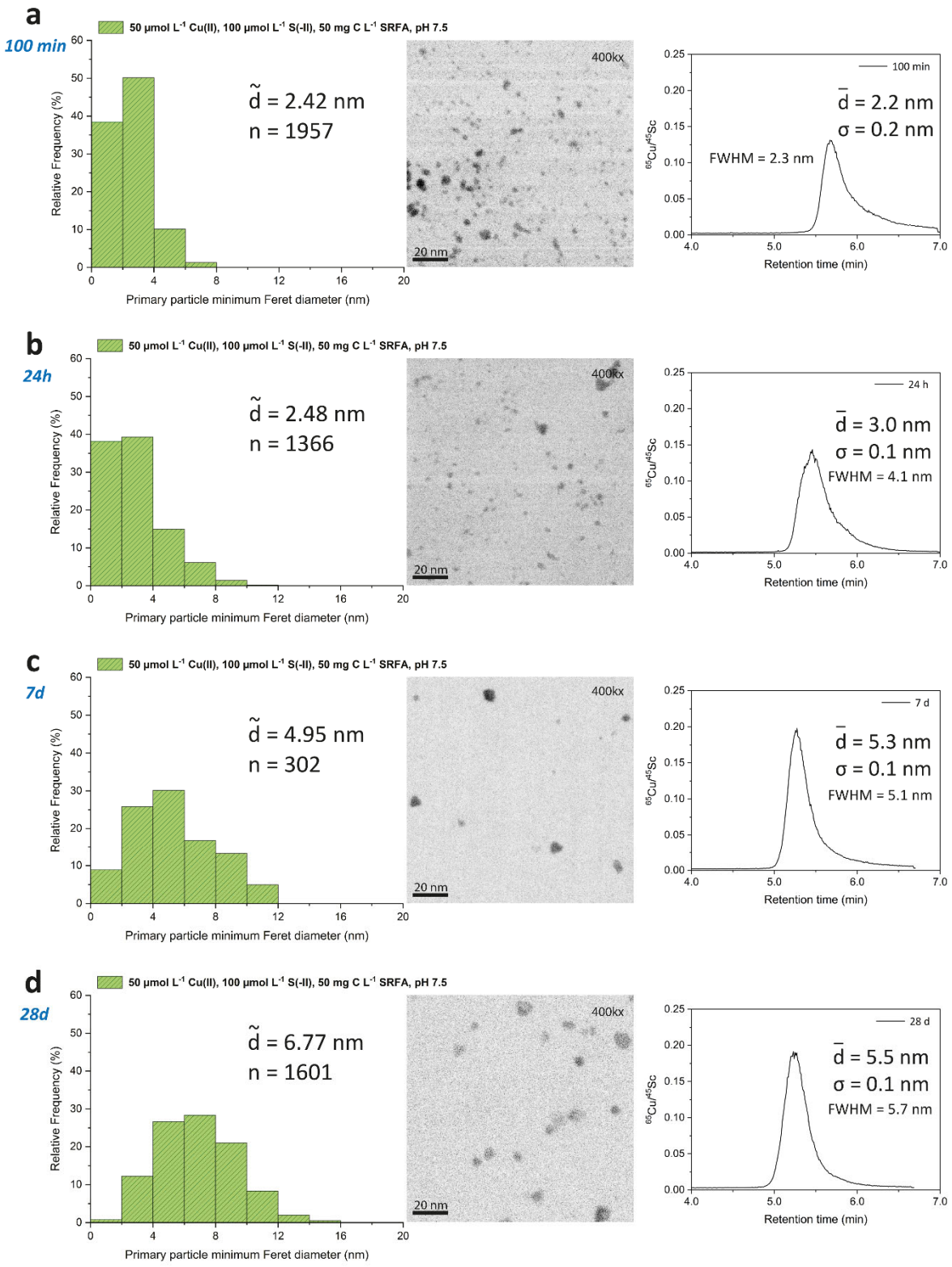

Figure S3: Particle size distributions (PSD) of Cu_xS particles (left panels) from dilute (50 µmol L^{-1} Cu(II), 100 µmol L^{-1} S(-II)) suspensions (at pH 7.5 and an ionic strength of 10 mmol L^{-1} NaCl) derived from TEM images (middle panels) in the presence of 50 mg C L^{-1} SRFA after 100 min (a), 24 h (b), 7 d (c) and 28 d (d) with median TEM diameters ($\tilde{d}$) and number of counted particles (n). HAADF-TEM images (shown as inverted images in the middle panels) show Cu_xS nanoparticles from corresponding suspensions. Size exclusion chromatograms of these suspensions (internal standard corrected ^{65}Cu signal displayed as intensity values) show retention time shifts in the course of the growth experiment with converted average SEC diameters ($\bar{d}$), standard deviation (σ) of triplicate samples (n=3) and full width at half maximum (FWHM).

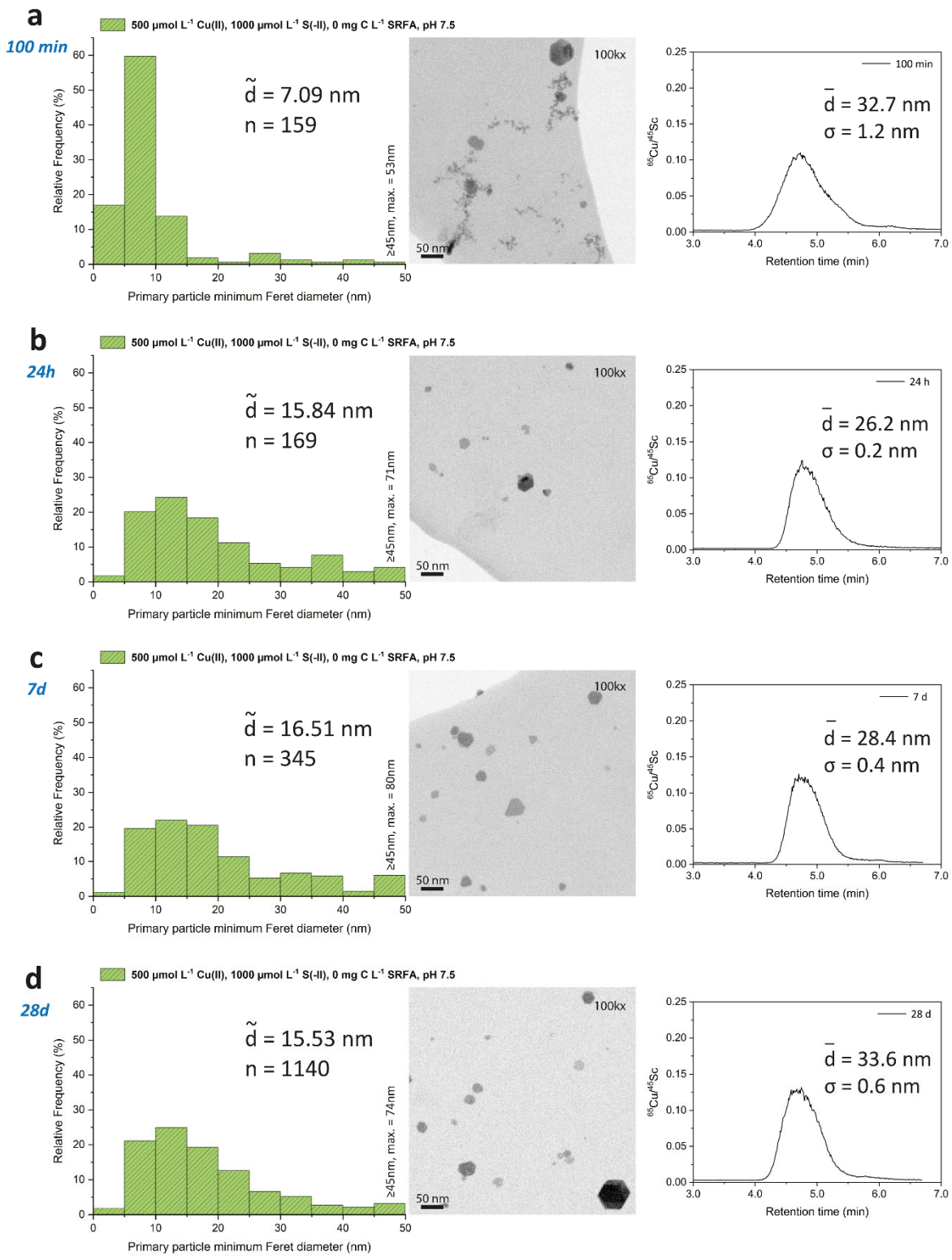

Figure S4: Particle size distributions (PSD) of Cu_xS particles (left panels) from concentrated (500 µmol L^{-1} Cu(II), 1000 µmol L^{-1} S(-II)) suspensions (at pH 7.5 and an ionic strength of 10 mmol L^{-1} NaCl) derived from TEM images (middle panels) absent in SRFA (0 mg C L^{-1}) after 100 min (a), 24 h (b), 7 d (c) and 28 d (d) with median TEM diameters ($\tilde{d}$) and number of counted particles (n). Counted particles larger than the given PSD limits were binned within the largest shown size bin, with size of the largest particle indicated (max.). HAADF-TEM images (shown as inverted images in the middle panels) show Cu_xS nanoparticles from corresponding suspensions. Size exclusion chromatograms of these suspensions (internal standard corrected ^{65}Cu signal displayed as intensity values) show retention time shifts in the course of the growth experiment with converted average SEC diameters ($\bar{d}$) and standard deviation (σ) of triplicate samples (n=3).

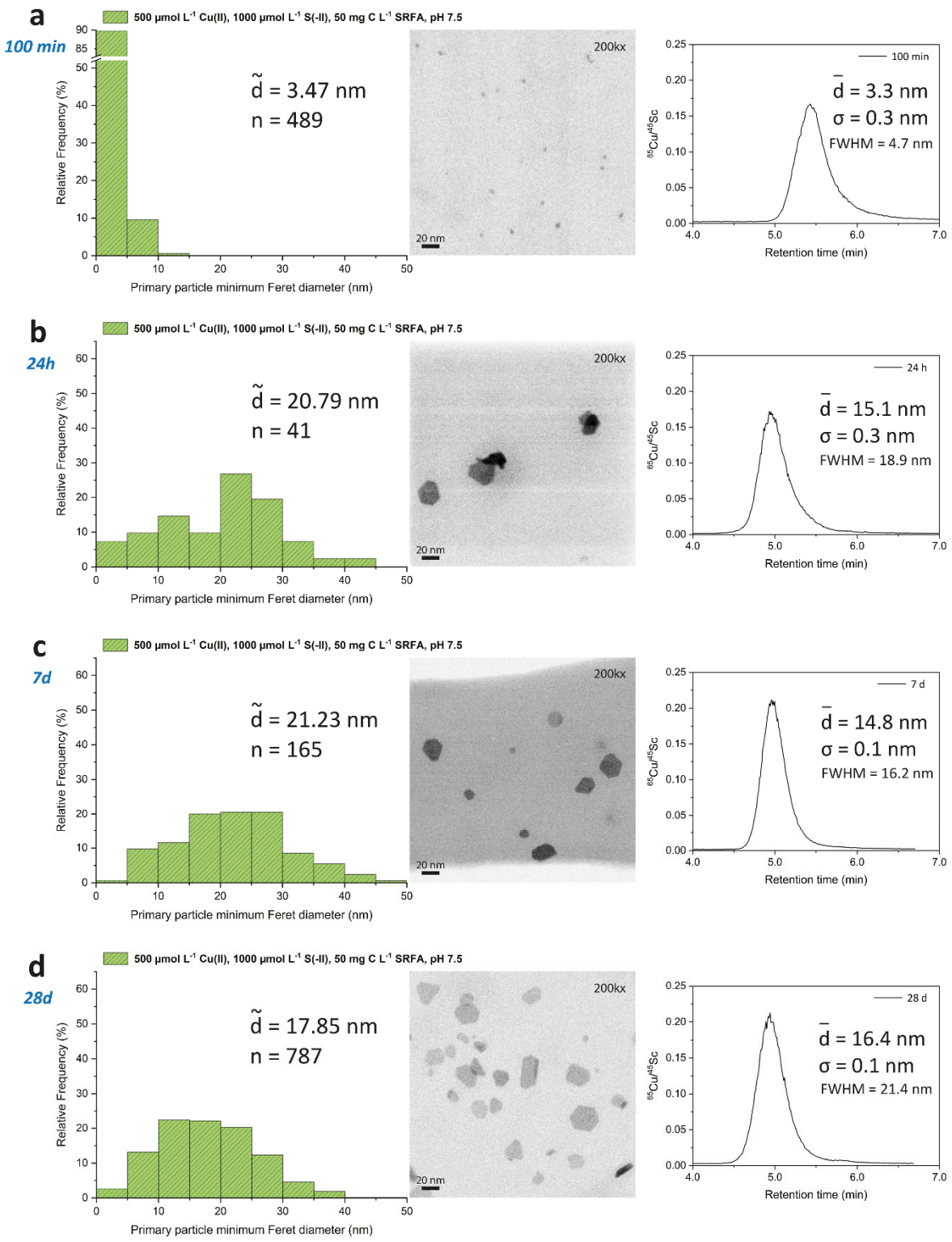

Figure S5: Particle size distributions (PSD) of Cu_xS particles (left panels) from concentrated (500 µmol L^{-1} Cu(II), 1000 µmol L^{-1} S(-II)) suspensions (at pH 7.5 and an ionic strength of 10 mmol L^{-1} NaCl) derived from TEM images (middle panels) in the presence of 50 mg C L^{-1} SRFA after 100 min (a), 24 h (b), 7 d (c) and 28 d (d) with median TEM diameters ($\tilde{d}$) and number of counted particles (n). HAADF-TEM images (shown as inverted images in the middle panels) show Cu_xS nanoparticles from corresponding suspensions. Size exclusion chromatograms of these suspensions (internal standard corrected ^{65}Cu signal displayed as intensity values) show retention time shifts in the course of the growth experiment with converted average SEC diameters ($\bar{d}$), standard deviation (σ) of triplicate samples (n=3) and full width at half maximum (FWHM).

Table S1: Summary of SEC and ICP-MS instrumental parameters used in the Cu_xS growth experiments.

SEC parameters	
Column	Macherey-Nagel Nucleosil-SiOH, 1000 Å and 4000 Å pore size, 250 x 4.6 mm, 5 µm particle size
Column temperature	25 °C
Flow rate	0.5 mL min^{-1}
Injection volume	50 µL
Mobile phase composition	0.5 % FL-70, 10 mmol L^{-1} NH_4NO_3
ICP-MS instrumentation	
Instrument	Agilent 8800 ICP-MS (ICP-QQQ)
Nebulizer type	Conikal
Sampler cone material	Platinum
Skimmer cone material	Platinum
ICP-MS parameters for analysis of AuNPs	
RF power	1500 W
Sampling depth	8 mm
Optional gas (20 % O_2 in Ar)	0.1 L min^{-1}
Carrier gas	1.0 L min^{-1} Ar
Cell gas	5 mL min^{-1} H_2
Monitored isotopes (m/z)	$^{45}Sc^+$, $^{89}Y^+$, $^{197}Au^+$
Integration time	0.1 s
ICP-MS parameters for analysis of Cu_xS NPs	
RF power	1500 W
Sampling depth	8 mm
Optional gas (20 % O_2 in Ar)	0.1 L min^{-1}
Carrier gas	1.0 L min^{-1} Ar
Cell gas	1 mL min^{-1} H_2 + 30 % O_2
Monitored isotopes (m/z)	$^{48}SO^+$, $^{61}ScO^+$, $^{65}Cu^+$, $^{105}YO^+$
Integration time	0.1 s

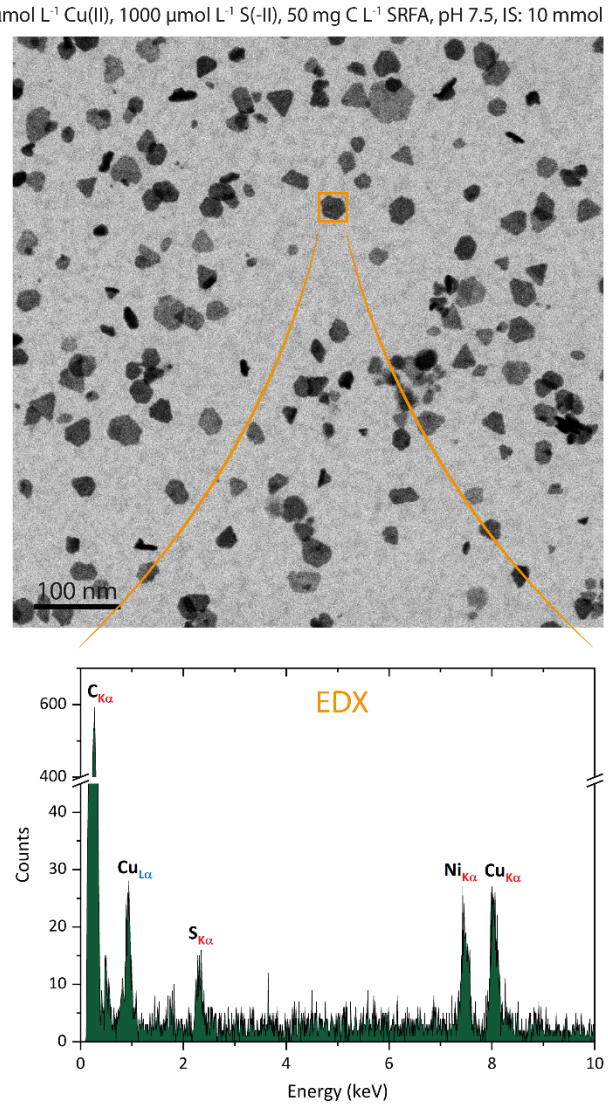

Figure S6: HAADF-TEM image (shown as inverted image) of concentrated (x10 reactants) Cu_xS suspensions in presence of 50 mg C L^{-1} fulvic acid after 24 h equilibration time. Background solutions consisted of 10 mmol L^{-1} NaCl at pH 7.5 (MOPS buffer). The bottom panel shows an EDX spectrum of a typical Cu_xS nanoparticle with hexagonal shape (marked particle). Peaks of Kα and Lα lines of the elements of interest are labelled.

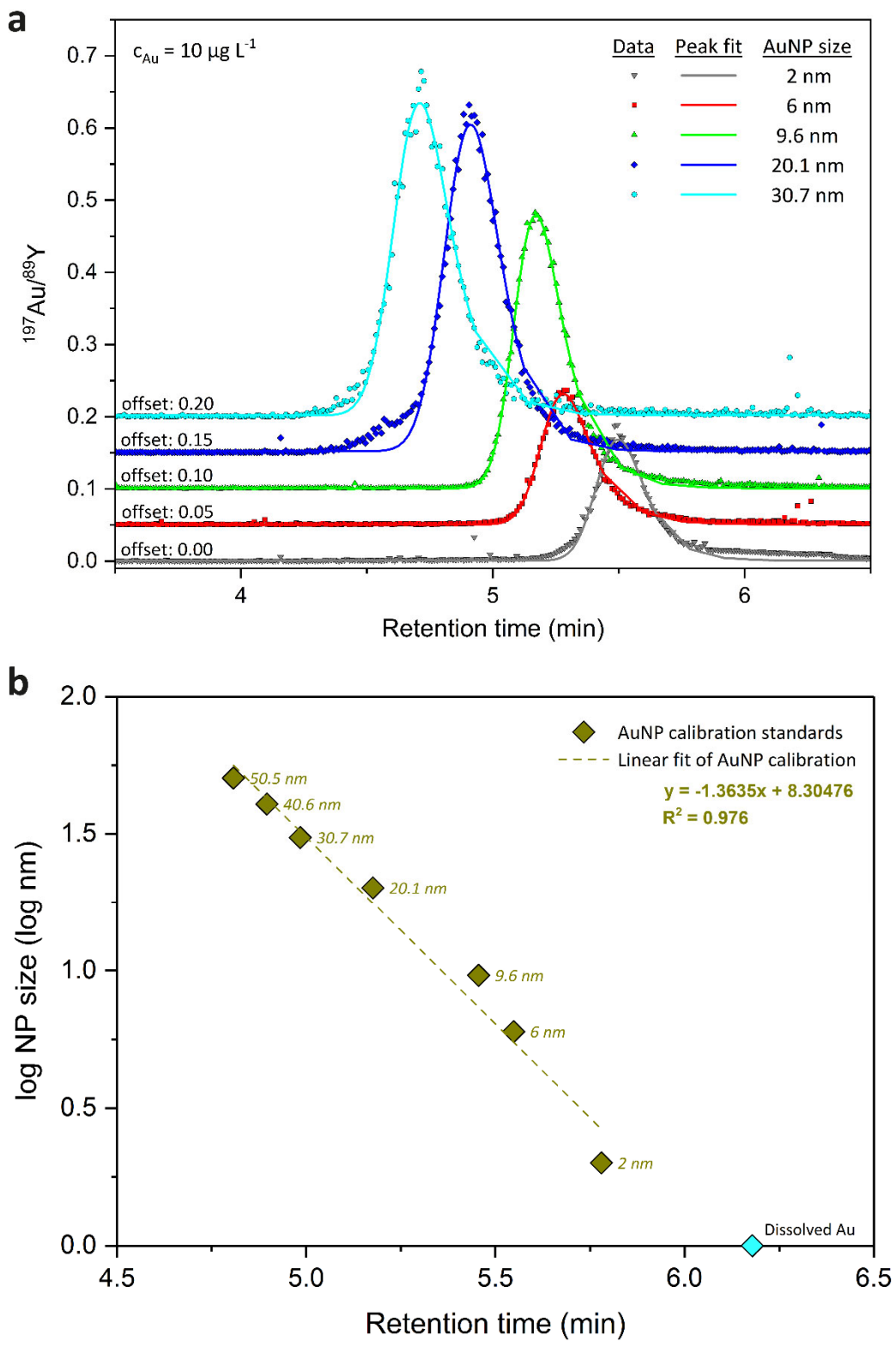

Figure S7: Size-exclusion chromatograms (a) of 10 µg L^{-1} injected Au nanoparticles of various sizes used for size calibration. Recorded data is shown as symbols and peaks fits are designated by lines. Typical AuNP size calibration (b) with linear fit (dashed line) and regression equation used for retention time to diameter conversion of the Cu_xS nanoparticle suspensions. Additionally, retention time of dissolved Au is depicted in order to show the limits of size detection.

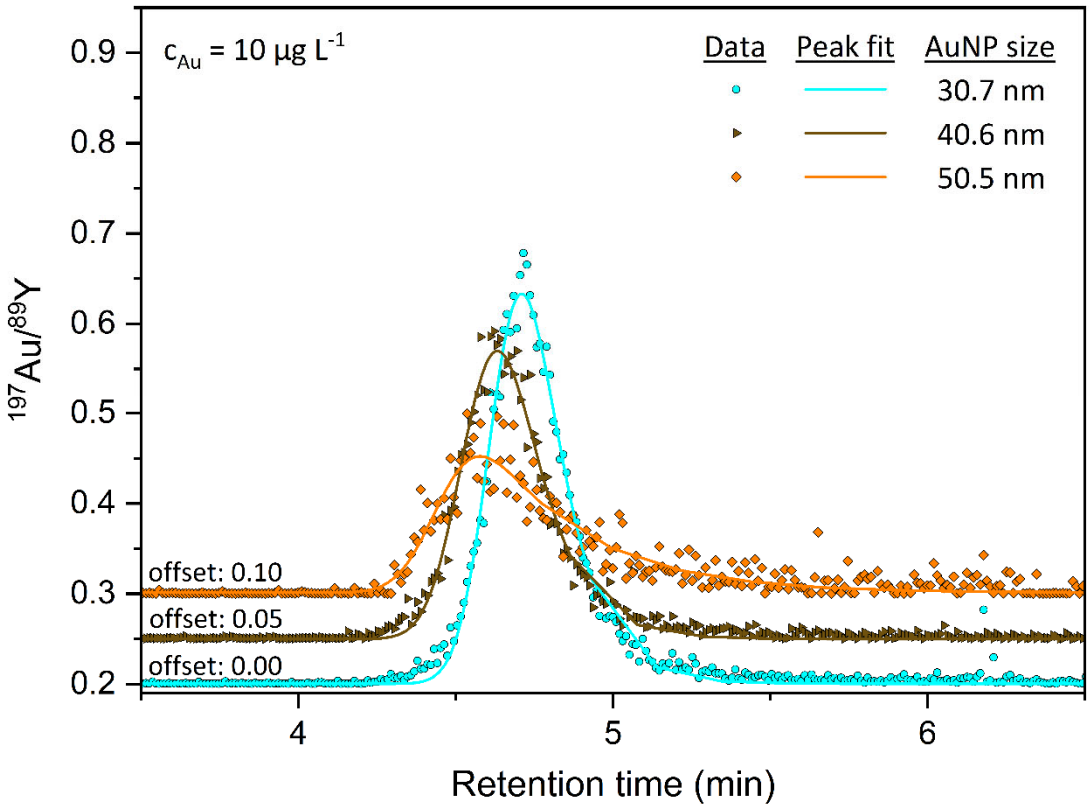

Figure S8: Size-exclusion chromatograms of 10 µg L^{-1} injected Au nanoparticles of 30 – 50 nm. Recorded data is shown as symbols and peaks fits are designated by lines.

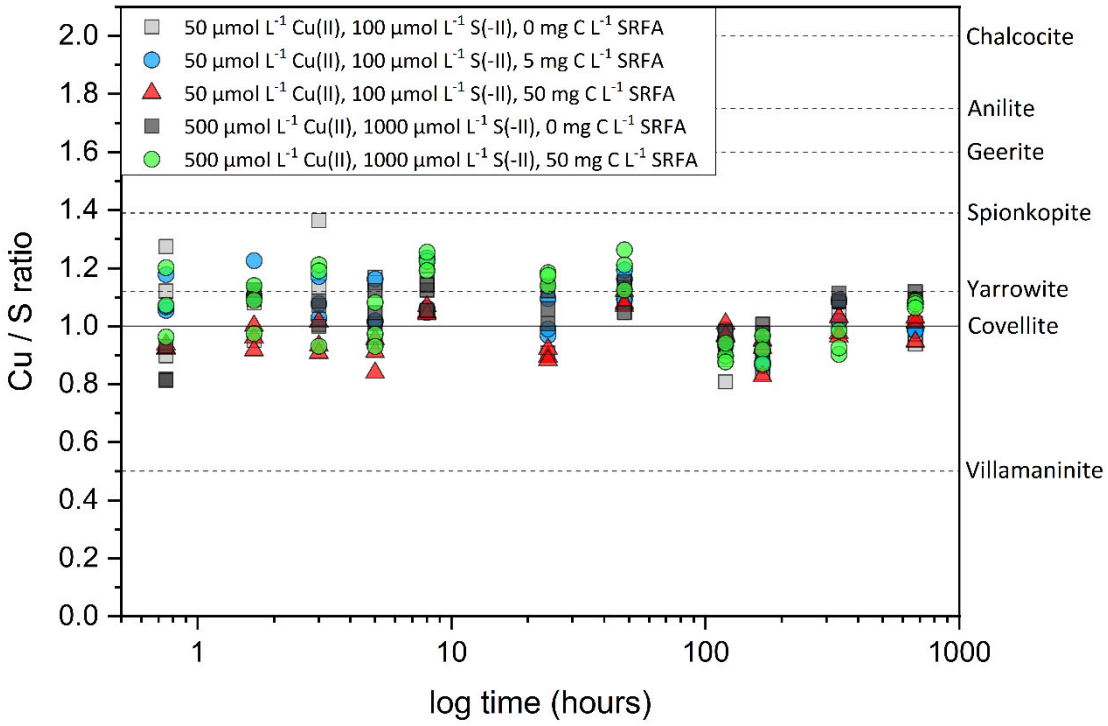

Figure S9: Cu : S ratios of all measured Cu_xS suspensions during the growth experiment. Respective Cu and S concentrations were calculated using chromatographic peak areas. Dashed lines delineate the theoretical Cu : S ratio within various copper sulfide minerals.

Table S2: Recoveries of AuNPs and Cu_xS nanoparticles at different instrumental conditions including the ones used in the growth experiments.

Au nanoparticles *MP = 0.5 % FL-70, 10 mmol L^{-1} NH_4NO_3, Q = 0.5 mL min^{-1}, 10 % O_2 option gas*	
Concentration & sample type	**Recovery**
10 ppb ionic Au	93%
10 ppb 2 nm AuNPs	82%
10 ppb 10 nm AuNPs	89%
10 ppb 20 nm AuNPs	88%
10 ppb 30 nm AuNPs	96%
10 ppb 40 nm AuNPs	110%
10 ppb 50 nm AuNPs	109%
Cu_xS nanoparticles *MP = 1 % FL-70, 10 mmol L^{-1} NH_4NO_3, Q = 0.5 mL min^{-1}*	
Concentration & sample type	
50 ppb Cu from: Cu(II) 50 µmol L^{-1}, S(-II) 100 µmol L^{-1}, 0 mg C L^{-1} SRFA	95%
50 ppb Cu from: Cu(II) 50 µmol L^{-1}, S(-II) 100 µmol L^{-1}, 5 mg C L^{-1} SRFA	101%
50 ppb Cu from: Cu(II) 50 µmol L^{-1}, S(-II) 100 µmol L^{-1}, 50 mg C L^{-1} SRFA	104%
50 ppb Cu from: Cu(II) 500 µmol L^{-1}, S(-II) 1000 µmol L^{-1}, 50 mg C L^{-1} SRFA	101%
MP = 0.5 % FL-70, 10 mmol L^{-1} NH_4NO_3, Q = 0.5 mL min^{-1}, 10 % O_2 option gas	
Concentration & sample type	
100 ppb ionic Cu	109%
100 ppb Cu from: Cu(II) 50 µmol L^{-1}, S(-II) 100 µmol L^{-1}, 0 mg C L^{-1} SRFA	96%
100 ppb Cu from: Cu(II) 500 µmol L^{-1}, S(-II) 1000 µmol L^{-1}, 50 mg C L^{-1} SRFA	101%

Composition: 50 µmol L^{-1} Cu(II), 100 µmol L^{-1} S(-II), 5 mg C L^{-1} SRFA, pH 6 (1 mmol L^{-1} MES buffer), IS: 10 mmol L^{-1} NaCl

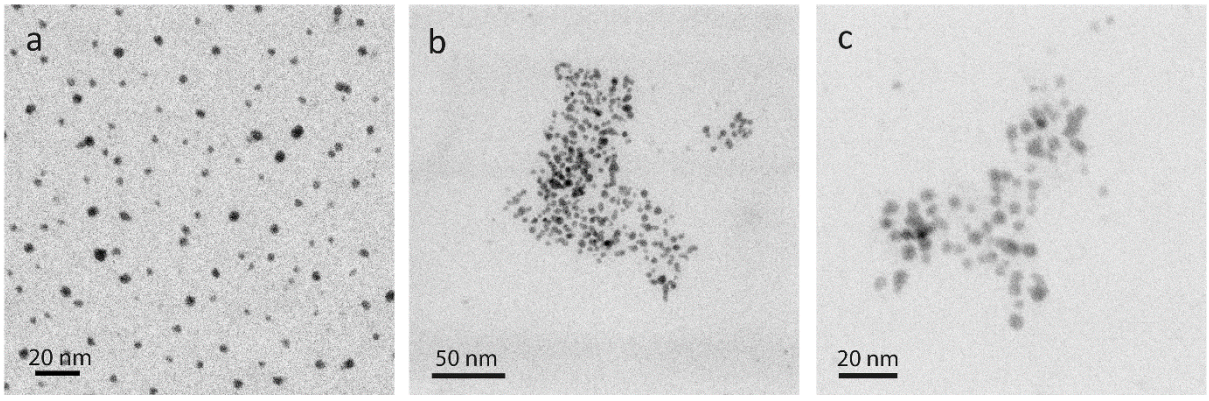

Figure S10: TEM images of a dilute Cu_xS suspension at pH 6 in the presence of 5 mg C L^{-1} fulvic acid at different magnifications after 24 h equilibration time.

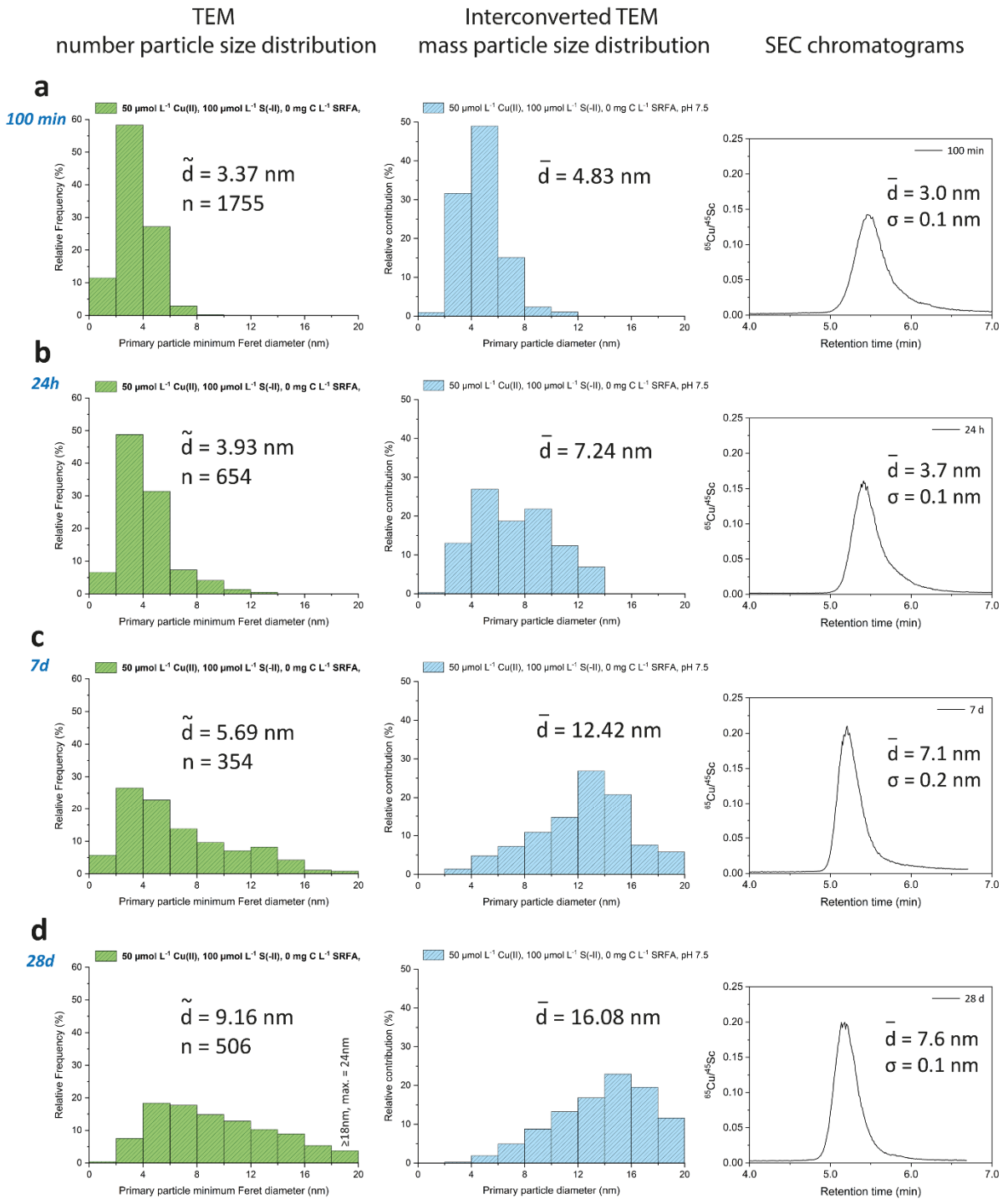

Figure S11: Number-based particle size distributions (left panels) of Cu_xS particles from dilute (50 µmol L^{-1} Cu(II), 100 µmol L^{-1} S(-II)) suspensions (at pH 7.5 and an ionic strength of 10 mmol L^{-1} NaCl) derived from TEM images absent in SRFA (0 mg C L^{-1}) after 100 min (a), 24 h (b), 7 d (c) and 28 d (d) with number-based median TEM diameters ($\tilde{d}$) and number of counted particles (n). The middle panel shows the *calculated* mass-based TEM particle size distributions and mass-based average TEM diameters ($\bar{d}$) of Cu_xS particles converted from the respective number-based TEM particle size distributions shown in the left panels assuming spherical particle shapes. Size exclusion chromatograms of these suspensions (internal standard corrected ^{65}Cu signal displayed as intensity values) are shown in the right panels with average SEC diameters ($\bar{d}$) and standard deviation (σ) of triplicate samples (n=3). The number particle size distributions and the SEC chromatograms are taken from Figure S1 and replotted for the sake of better comparison with *calculated* mass-based TEM particle size distributions and diameters.

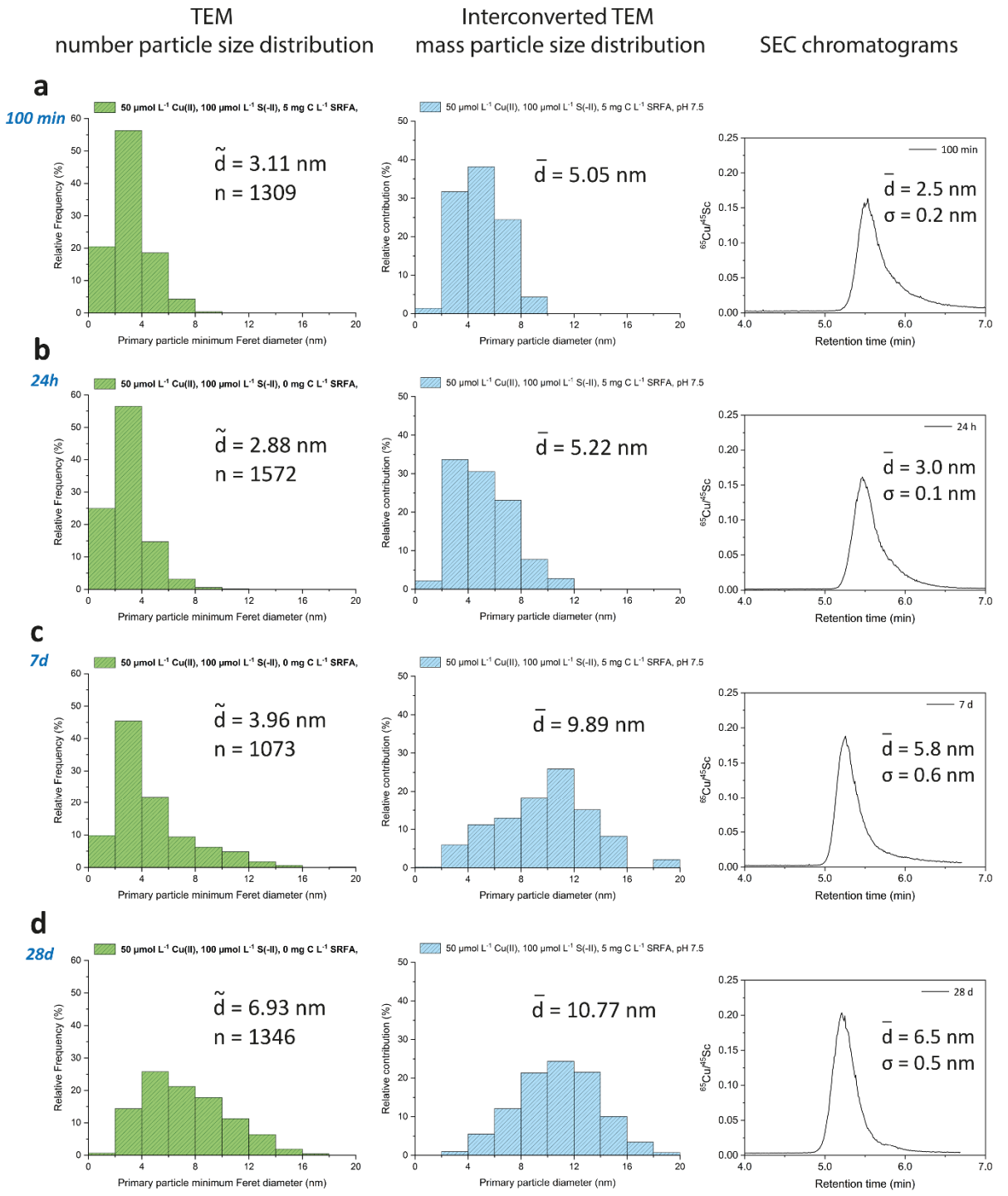

Figure S12: Number-based particle size distributions (left panels) of Cu_xS particles from dilute (50 µmol L^{-1} Cu(II), 100 µmol L^{-1} S(-II)) suspensions (at pH 7.5 and an ionic strength of 10 mmol L^{-1} NaCl) derived from TEM images in the presence of 5 mg C L^{-1} SRFA after 100 min (a), 24 h (b), 7 d (c) and 28 d (d) with number-based median TEM diameters ($\tilde{d}$) and number of counted particles (n). The middle panel shows the *calculated* mass-based TEM particle size distributions and mass-based average TEM diameters ($\bar{d}$) of Cu_xS particles converted from the respective number-based TEM particle size distributions shown in the left panels assuming spherical particle shapes. Size exclusion chromatograms of these suspensions (internal standard corrected ^{65}Cu signal displayed as intensity values) are shown in the right panels with average SEC diameters ($\bar{d}$) and standard deviation (σ) of triplicate samples (n=3). The number particle size distributions and the SEC chromatograms are taken from Figure S2 and replotted for the sake of better comparison with *calculated* mass-based TEM particle size distributions and diameters.

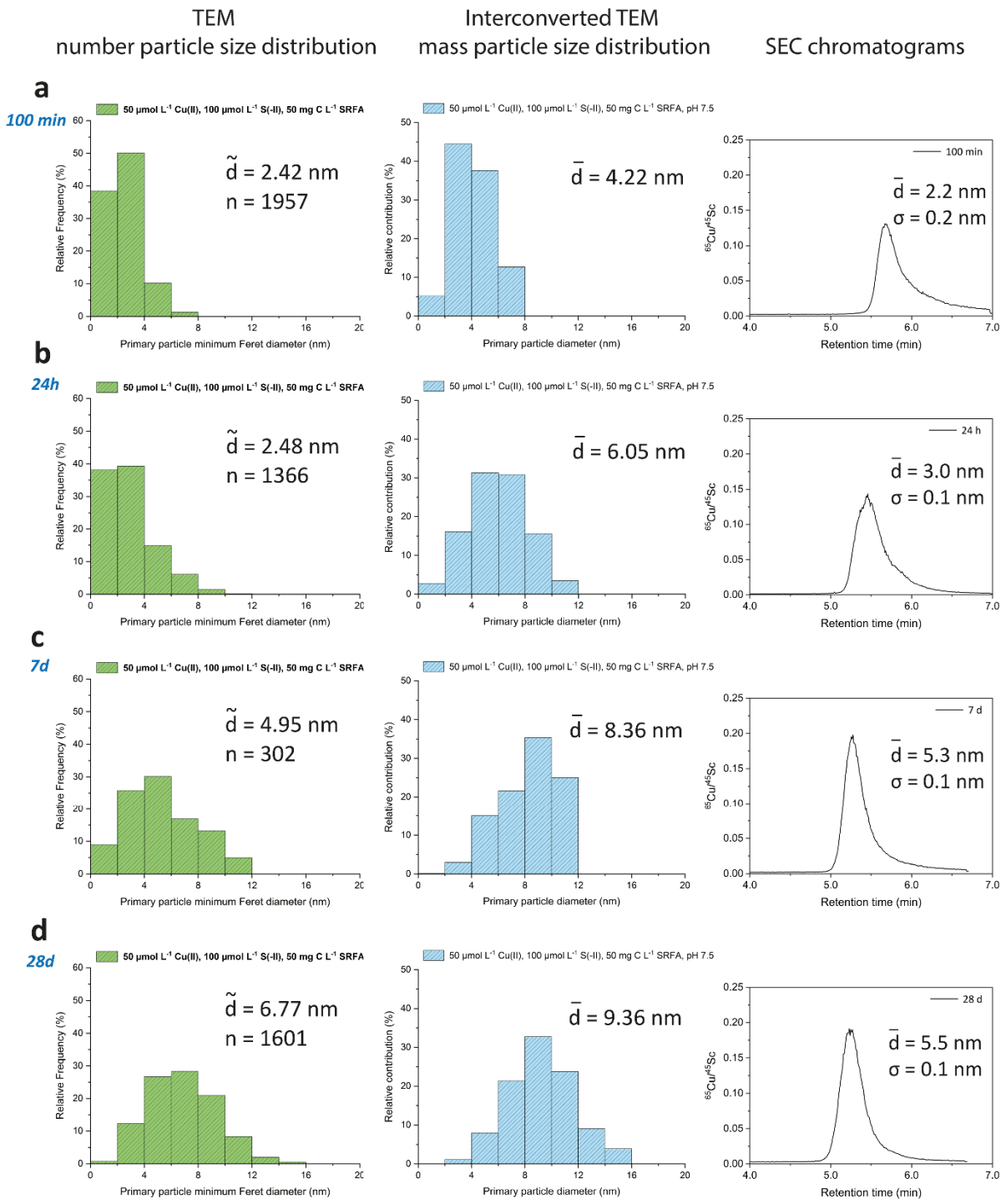

Figure S13: Number-based particle size distributions (left panels) of Cu_xS particles from dilute (50 µmol L^{-1} Cu(II), 100 µmol L^{-1} S(-II)) suspensions (at pH 7.5 and an ionic strength of 10 mmol L^{-1} NaCl) derived from TEM images in the presence of 50 mg C L^{-1} SRFA after 100 min (a), 24 h (b), 7 d (c) and 28 d (d) with number-based median TEM diameters ($\tilde{d}$) and number of counted particles (n). The middle panel shows the *calculated* mass-based TEM particle size distributions and mass-based average TEM diameters ($\bar{d}$) of Cu_xS particles converted from the respective number-based TEM particle size distributions shown in the left panels assuming spherical particle shapes. Size exclusion chromatograms of these suspensions (internal standard corrected ^{65}Cu signal displayed as intensity values) are shown in the right panels with average SEC diameters ($\bar{d}$) and standard deviation (σ) of triplicate samples (n=3). The number particle size distributions and the SEC chromatograms are taken from Figure S3 and replotted for the sake of better comparison with *calculated* mass-based TEM particle size distributions and diameters.

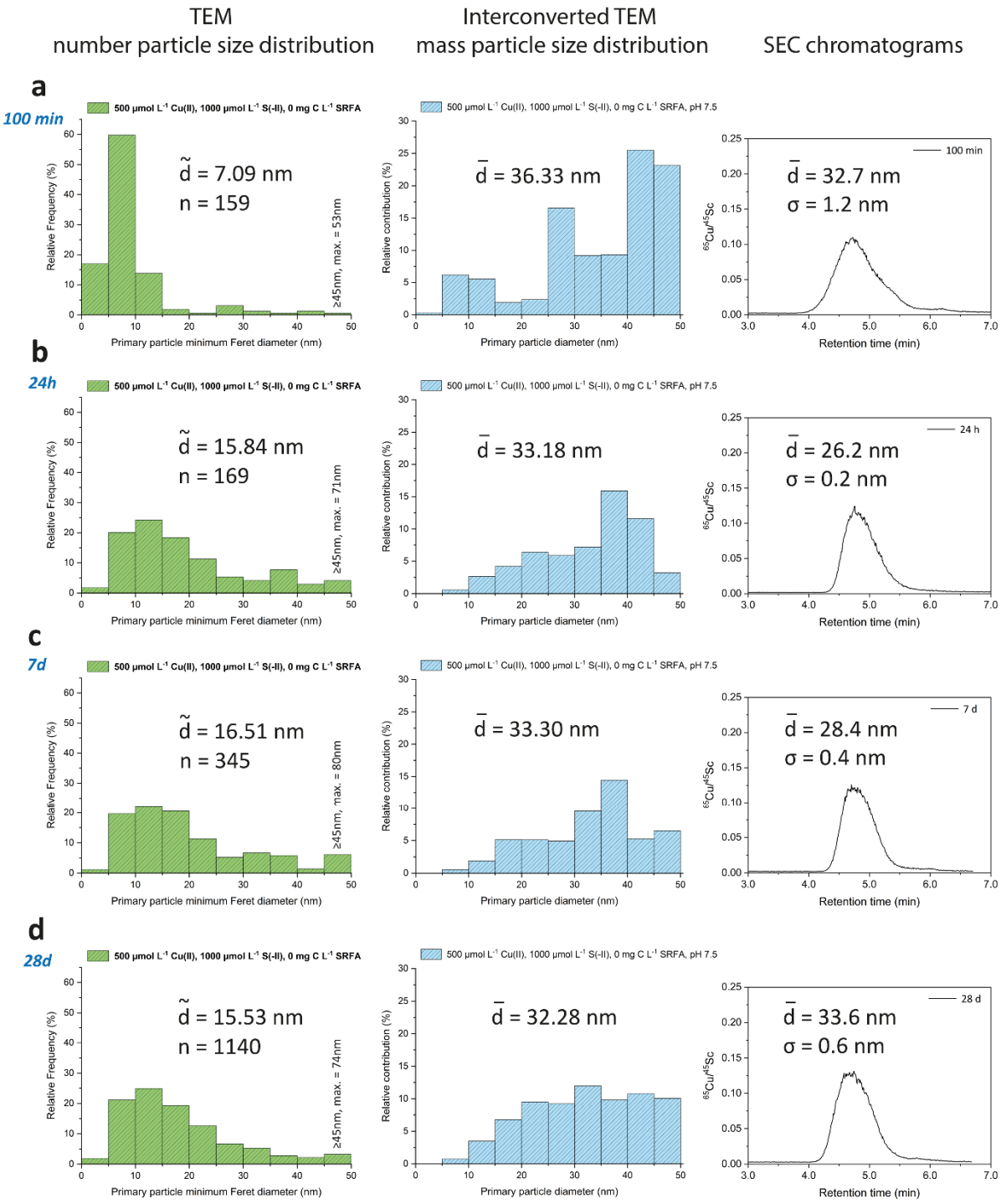

Figure S14: Number-based particle size distributions (left panels) of Cu_xS particles from concentrated (500 µmol L^{-1} Cu(II), 1000 µmol L^{-1} S(-II)) suspensions (at pH 7.5 and an ionic strength of 10 mmol L^{-1} NaCl) derived from TEM images absent in SRFA (0 mg C L^{-1}) after 100 min (a), 24 h (b), 7 d (c) and 28 d (d) with number-based median TEM diameters ($\tilde{d}$) and number of counted particles (n). The middle panel shows the *calculated* mass-based TEM particle size distributions and mass-based average TEM diameters ($\bar{d}$) of Cu_xS particles converted from the respective number-based TEM particle size distributions shown in the left panels assuming spherical particle shapes. Size exclusion chromatograms of these suspensions (internal standard corrected ^{65}Cu signal displayed as intensity values) are shown in the right panels with average SEC diameters ($\bar{d}$) and standard deviation (σ) of triplicate samples (n=3). The number particle size distributions and the SEC chromatograms are taken from Figure S4 and replotted for the sake of better comparison with *calculated* mass-based TEM particle size distributions and diameters.

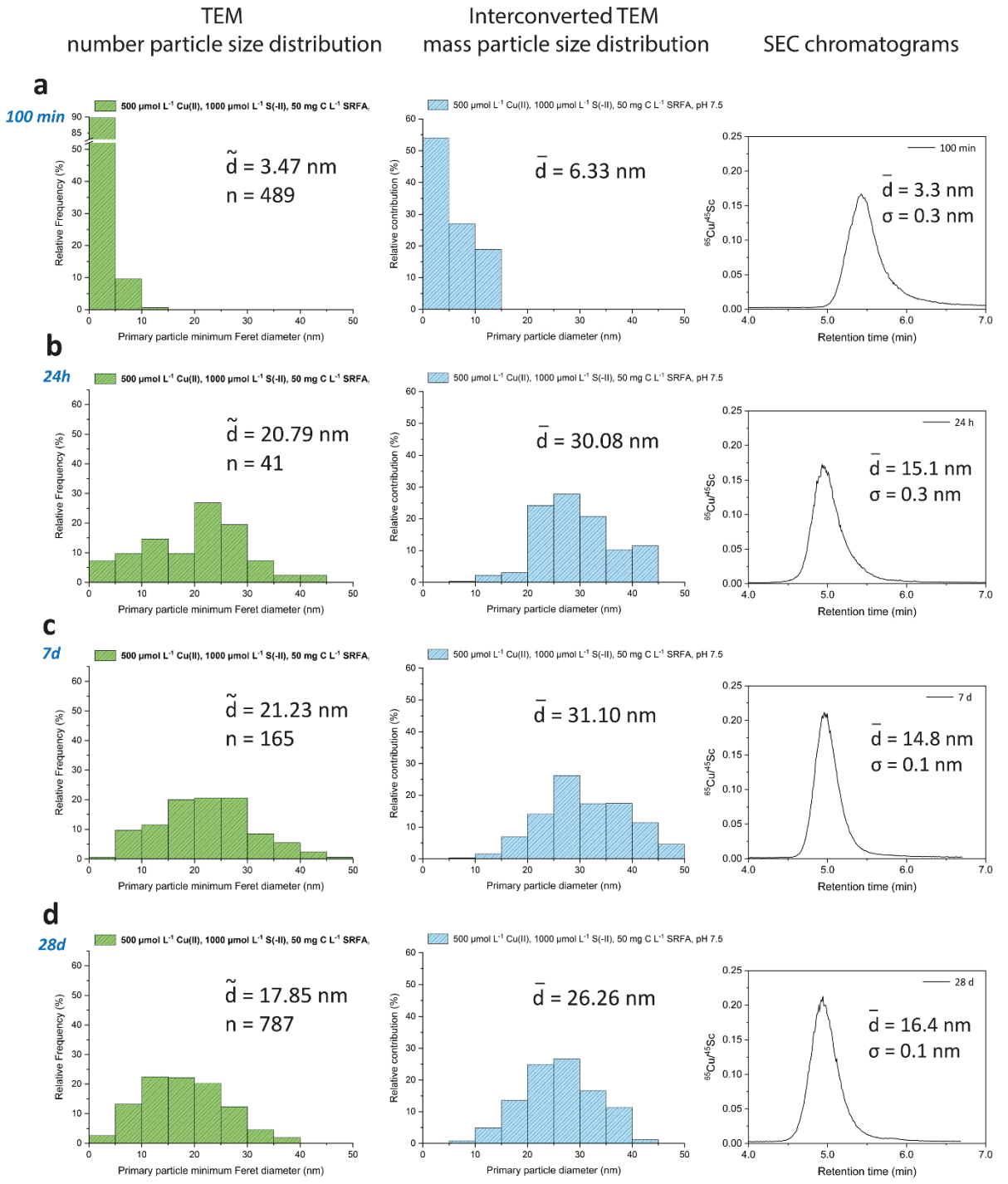

Figure S15: Number-based particle size distributions (left panels) of Cu_xS particles from concentrated (500 µmol L^{-1} Cu(II), 1000 µmol L^{-1} S(-II)) suspensions (at pH 7.5 and an ionic strength of 10 mmol L^{-1} NaCl) derived from TEM images in the presence of 50 mg C L^{-1} SRFA after 100 min (a), 24 h (b), 7 d (c) and 28 d (d) with number-based median TEM diameters ($\tilde{d}$) and number of counted particles (n). The middle panel shows the *calculated* mass-based TEM particle size distributions and mass-based average TEM diameters ($\bar{d}$) of Cu_xS particles converted from the respective number-based TEM particle size distributions shown in the left panels assuming spherical particle shapes. Size exclusion chromatograms of these suspensions (internal standard corrected ^{65}Cu signal displayed as intensity values) are shown in the right panels with average SEC diameters ($\bar{d}$) and standard deviation (σ) of triplicate samples (n=3). The number particle size distributions and the SEC chromatograms are taken from Figure S5 and replotted for the sake of better comparison with *calculated* mass-based TEM particle size distributions and diameters.

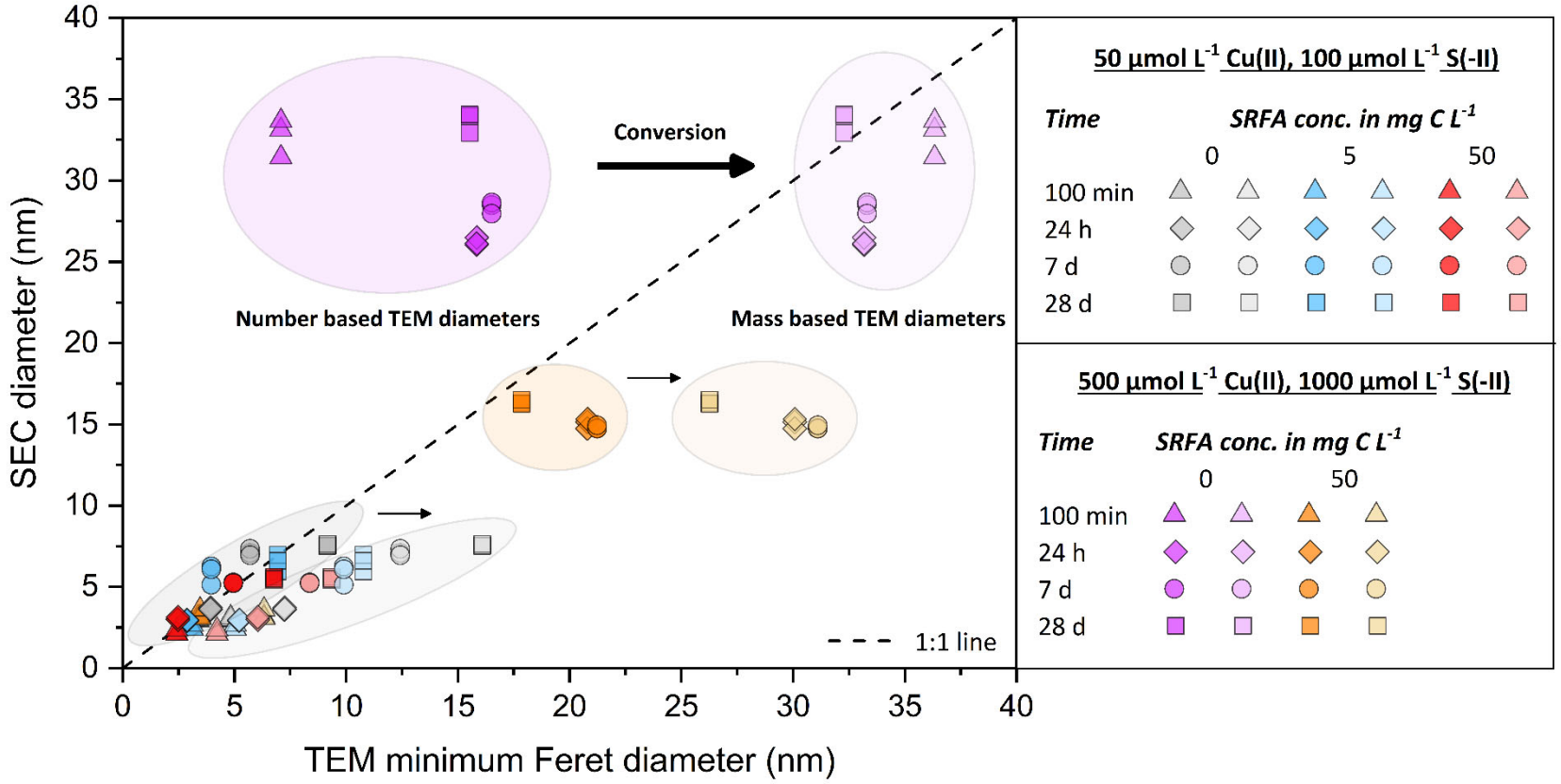

Figure S16: This figure constitutes a modified and extended representation of Figure 3c. It shows a regression plot of SEC diameter values measured during the Cu_xS growth experiment (after 100 min, 1 d, 7 d and 28 d) from various suspensions, the corresponding number-based median TEM diameters of the same samples (more intensely colored symbols) and the added *calculated* mass-based average TEM diameters (brighter colored symbols) which were converted from the respective number-based TEM particle size distributions shown in Figures S1-S5 assuming spherical particle shapes. The dashed line signifies the 1:1 line indicating 100 % conformity of SEC and TEM sizes. In all cases, the ionic strength (IS) was 10 mmol L^{-1} NaCl.

Composition: 500 µmol L^{-1} Cu(II), 1000 µmol L^{-1} S(-II), 0 mg C L^{-1} SRFA, pH 7.5, IS: 10 mmol L^{-1} NaCl

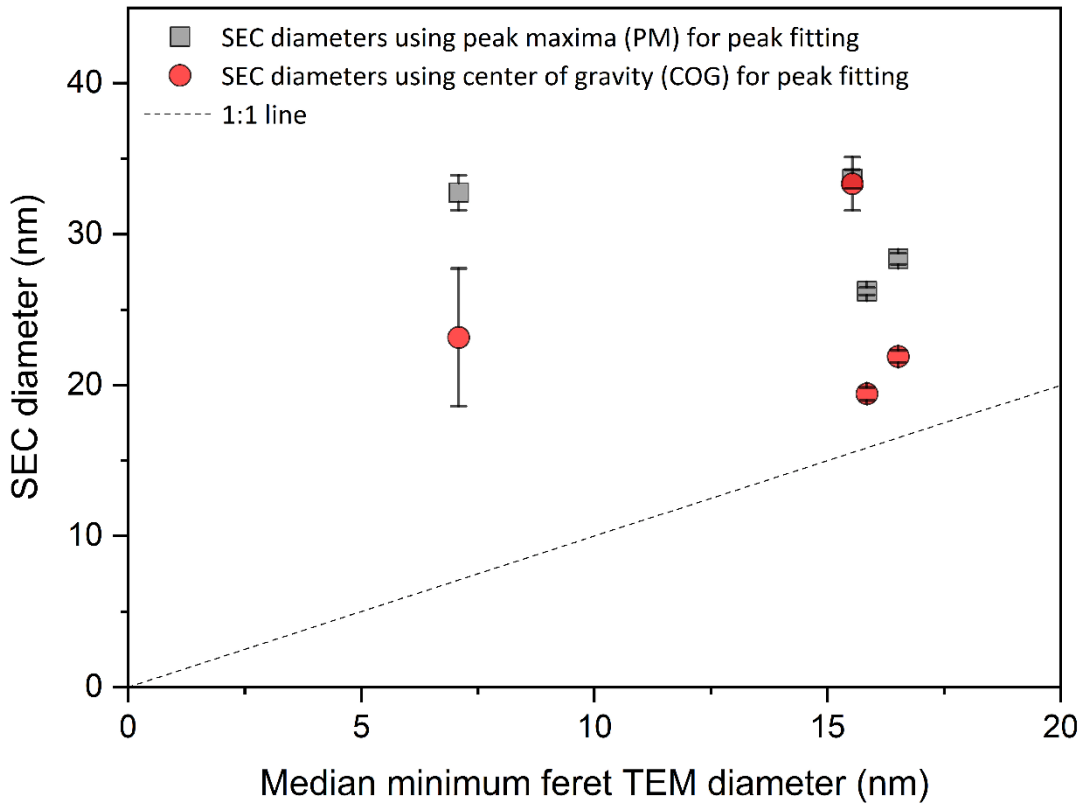

Figure S17: Comparison of converted SEC diameters using the peak maxima (PM) vs. center of gravity (COG) for peak fitting and relation to median minimum Feret TEM diameters in concentrated, SRFA-free suspensions.

Table S3: Comparison of SEC diameters derived from using peak maxima (PM) vs. center of gravity (COG) for peak fitting from the Cu_xS growth experiment over 4 weeks for dilute suspensions.

	Experimental time (h)	Diameters (nm) derived from **peak maxima**	Std.Dev. (nm)	Diameters (nm) derived from **center of gravity**	Std.Dev. (nm)
50 µmol L^{-1} Cu(II), 100 µmol L^{-1} S(-II), No SRFA	0.75	3.0	0.07	2.4	0.19
	1.67	3.0	0.10	2.4	0.16
	3	3.3	0.06	2.7	0.15
	5	3.4	0.29	2.7	0.31
	8	3.5	0.03	2.9	0.02
	24	3.7	0.06	2.9	0.05
	48	3.9	0.21	3.7	0.32
	120	6.3	0.31	4.7	0.34
	168	7.1	0.20	6.1	0.31
	336	7.0	0.15	6.3	0.15
	672	7.6	0.06	7.2	0.09
50 µmol L^{-1} Cu(II), 100 µmol L^{-1} S(-II), 5 mg C L^{-1} SRFA	0.75	2.3	0.12	1.6	0.17
	1.67	2.5	0.15	1.7	0.14
	3	2.7	0.11	1.8	0.18
	5	2.9	0.09	2.0	0.17
	8	2.8	0.07	2.0	0.07
	24	3.0	0.02	2.2	0.06
	48	3.3	0.38	2.8	0.18
	120	5.2	0.82	3.7	0.74
	168	5.8	0.61	4.6	0.73
	336	6.1	0.55	5.3	0.61
	672	6.5	0.53	6.0	0.53
50 µmol L^{-1} Cu(II), 100 µmol L^{-1} S(-II), 50 mg C L^{-1} SRFA	0.75	2.1	0.10	1.3	0.09
	1.67	2.2	0.15	1.4	0.14
	3	2.4	0.11	1.5	0.14
	5	2.5	0.06	1.6	0.16
	8	2.5	0.01	1.8	0.02
	24	3.0	0.09	2.3	0.05
	48	4.1	0.13	3.2	0.13
	120	5.0	0.08	3.7	0.01
	168	5.3	0.02	4.2	0.03
	336	5.7	0.07	4.9	0.04
	672	5.5	0.10	5.0	0.07

Table S4: Comparison of SEC diameters derived from using peak maxima (PM) vs. center of gravity (COG) for peak fitting from the Cu_xS growth experiment over 4 weeks for concentrated suspensions.

	Experimental time (h)	Diameters (nm) derived from **peak maxima**	Std.Dev. (nm)	Diameters (nm) derived from **center of gravity**	Std.Dev. (nm)
500 µmol L^{-1} Cu(II), 1000 µmol L^{-1} S(-II), No SRFA	0.75	39.9	2.46	23.1	7.46
	1.67	32.7	1.17	23.2	4.56
	3	28.9	0.49	20.1	2.46
	5	26.7	1.41	19.7	2.65
	8	29.8	0.78	17.7	0.70
	24	26.2	0.24	19.4	0.44
	48	31.6	0.55	25.5	0.61
	120	30.8	0.62	23.7	0.29
	168	28.4	0.36	21.9	0.40
	336	29.3	0.25	25.4	0.53
	672	33.6	0.63	33.3	1.77
500 µmol L^{-1} Cu(II), 1000 µmol L^{-1} S(-II), 50 mg C L^{-1} SRFA	0.75	3.0	0.22	2.4	0.22
	1.67	3.3	0.29	2.8	0.29
	3	3.4	0.27	3.0	0.30
	5	6.1	2.59	3.5	0.87
	8	15.5	0.15	12.9	0.17
	24	15.1	0.30	12.9	0.44
	48	14.4	0.09	13.4	0.18
	120	14.3	0.23	12.4	0.23
	168	14.8	0.11	13.2	0.18
	336	14.4	0.21	13.5	0.31
	672	16.4	0.13	16.7	0.17

Composition: 500 µmol L^{-1} Cu(II), 1000 µmol L^{-1} S(-II), 50 mg C L^{-1} SRFA, pH 7.5, IS: 10 mmol L^{-1} NaCl

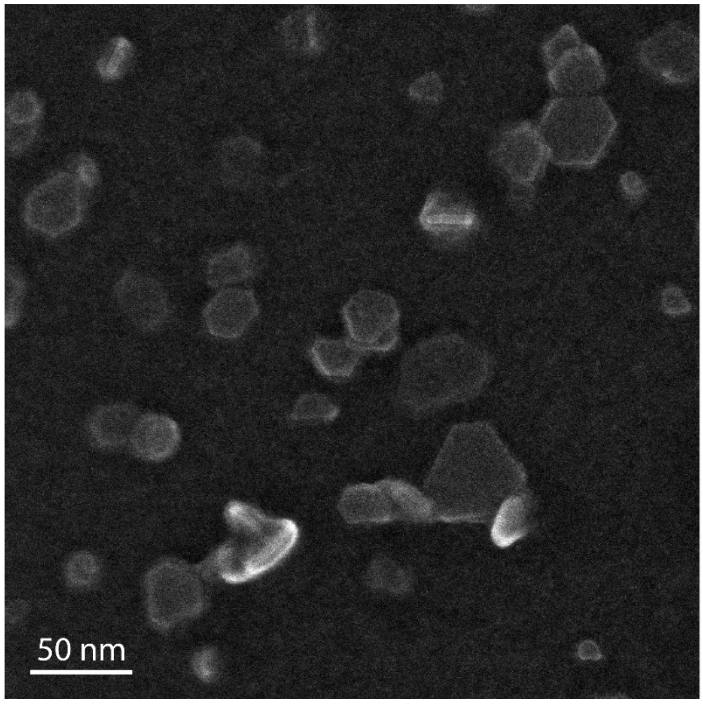

Figure S18: SEM image showing hexagonal Cu_xS platelets standing upright on the grid or partly lying above each other in concentrated suspensions containing 50 mg C L^{-1} SRFA after 4 weeks of aging.

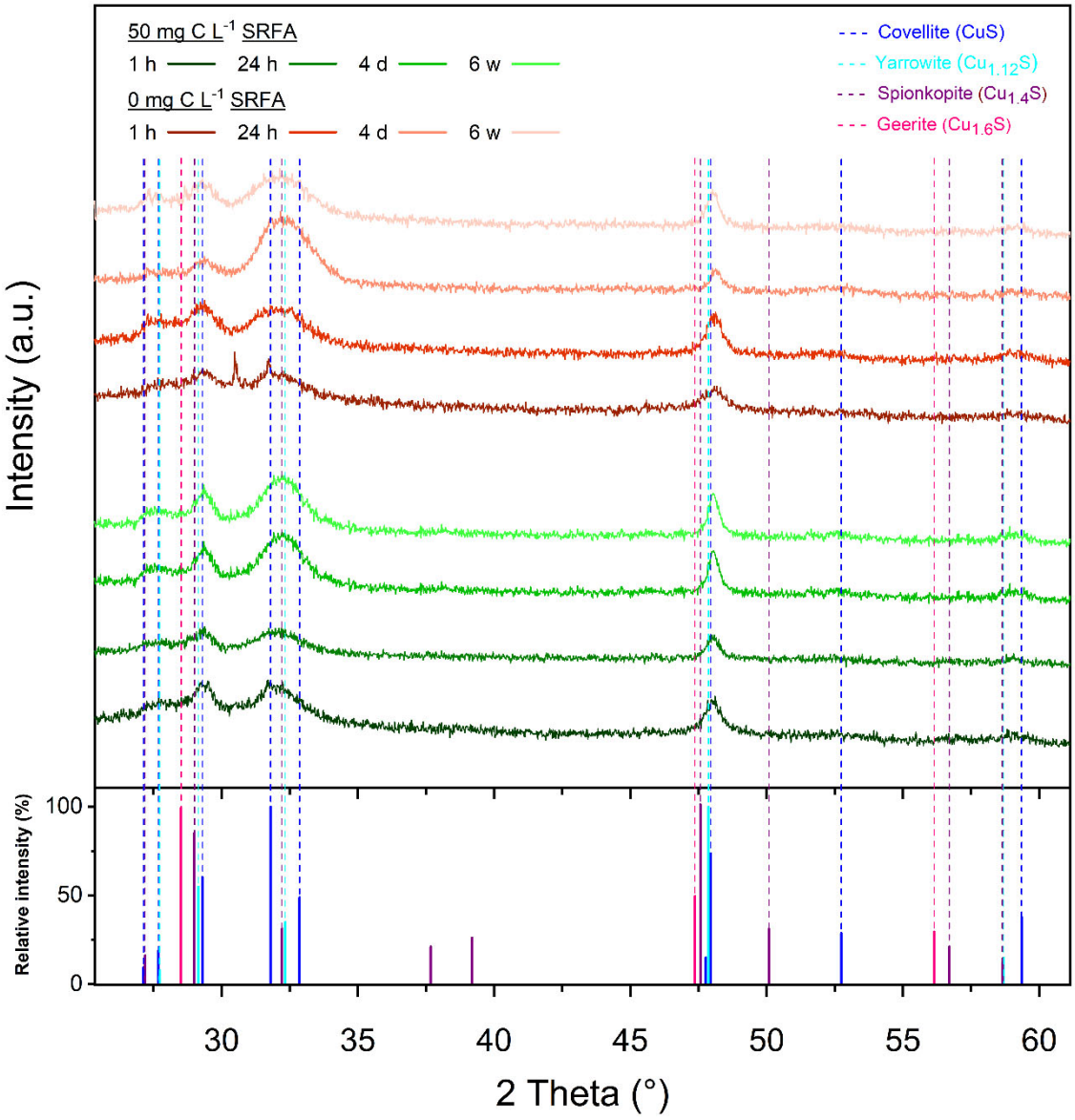

Figure S19: Diffractograms of different concentrated Cu_xS suspensions at different times of aging (1 h, 24 h, 4 d, 6 weeks) in the absence and presence of 50 mg C L^{-1} fulvic acid. The bottom part of the figure shows the major reflections (with their relative intensities) of the Cu_xS phases covellite, yarrowite, spionkopite and geerite. Dashed lines originating from these reflections show the (qualitative) peak matching analysis with the recorded diffractograms.

Table S5: Electrophoretic mobilites and Zeta potentials with standard deviations for concentrated suspensions in the absence and presence of SRFA. Electrophoretic mobility measurements were conducted via laser doppler velocimetry combined with phase analysis light scattering (LDV-PALS, Nano ZS, Malvern Instruments, UK) to gather information on surface charge of the metal sulfides. Data were recorded in a minimum of six runs per aliquot, each comprising 22 individual measurements at an applied voltage of 150 V at 25°C. Electrophoretic mobility data were transformed into zeta potentials (ZP) by applying the Smoluchowski approximation model[1] with the Henry function F(κα) = 3/2 for aqueous media. Runs showing distorted phase plots were rejected.

Cu_xS nanoparticle surface charge

IS: 10 mmol L^{-1} NaCl, pH 7.5

Sample	Electrophoretic mobility (µmcm Vs^{-1})	Standard deviation (±µmcm Vs^{-1})	Zeta potential (mV)	Standard deviation (±mV)
Cu(II) 500 µmol L^{-1}, S(-II) 1000 µmol L^{-1}, 0 mg C L^{-1} SRFA	-3.9	0.2	-50.7	2.0
Cu(II) 500 µmol L^{-1}, S(-II) 1000 µmol L^{-1}, 50 mg C L^{-1} SRFA	-3.8	0.1	-49.8	1.3

Thermodynamic modelling with Visual MINTEQ

Speciation of different reagent mixtures used for the formation of Cu_xS nanoparticles was modelled with Visual MINTEQ 3.1[2] *before and after* sulfide addition. Default databases (component database: comp_2008.vdb, main thermodynamic database: thermo.vdb, solids database: type6.vdb, Gaussian DOM database: Gaussian.vdb) integrated in Visual MINTEQ were used. In order to account for Cu complexation on SRFA, the NICA-Donnan model was applied with the generalized parameters of Milne et al. (2003).[3] For activity corrections, we used the Davies equation with a b-parameter of 0.3. Oversaturated solids were allowed to precipitate in each iteration step. Gas equilibria were not included in the calculations. All calculations were performed at 25 °C. To account for reducing conditions in the glovebox, redox potential was fixed at Eh = -100 mV for all calculations.

Table S6: Speciation of reagent mixtures (a-e) used for formation of Cu_xS nanoparticles *before* sulfide addition as calculated with Visual MINTEQ 3.1. Reagent mixtures with different SRFA concentrations and absolute concentrations are presented.

a) 50 µmol L^{-1} Cu (II), 0 µmol L^{-1} S(-II), 0 mg C L^{-1} SRFA

Input

Species	Na^+ (mol L^{-1})	Cl^- (mol L^{-1})	MOPS (mol L^{-1})	SRFA (mg C L^{-1})	Cu(II) (µmol L^{-1})	pH
Concentration	0.01	0.01	0.001	0	50	7.5

Distribution of components between dissolved and precipitated species (in mol L^{-1})

Component	Total dissolved	% dissolved	Total precipitated	% precipitated
Cu(II)	8.07E-07	1.61	4.92E-05	98.39
Cl^-	9.98E-03	99.80	2.46E-05	0.25

Solids data

Mineral	Saturation index (= log IAP – log Ks)	Minerals precipitated	Equilibrium amount (mol L^{-1})
Atacamite	0	Atacamite	2.46E-05
$Cu(OH)_2(s)$	-0.821		

b) 50 µmol L^{-1} Cu (II), 0 µmol L^{-1} S(-II), 5 mg C L^{-1} SRFA

Input

Species	Na^+ (mol L^{-1})	Cl^- (mol L^{-1})	MOPS (mol L^{-1})	SRFA (mg C L^{-1})	Cu(II) (µmol L^{-1})	pH
Concentration	0.01	0.01	0.001	5	50	7.5

Distribution of components between dissolved and precipitated species (in mol L^{-1})

Component	Total dissolved	% dissolved	Dissolved inorganic	Bound to DOM	% bound to DOM	Total precipitated	% precipitated
Cu(II)	9.61E-06	19.21	8.07E-07	8.80E-06	91.6	4.04E-05	80.79
Cl^-	9.98E-03	99.80	9.98E-03	0	0	2.02E-05	0.2

Dissolved data

Component	% of total concentration	Species
Cu^{2+}	4.6	Cu+2
	26.4	FA2-Cu(6)(aq)
	3.4	CuOH+
	0.2	Cu(OH)2 (aq)
	0.1	Cu2(OH)2+2
	0.1	CuCl+
	1.4	(6)Cu+2D(aq)
	63.8	FA1-Cu(6)(aq)
HFA1-(6)(aq)	85.5	HFA1-(6)(aq)
	1.9	FA1-H(6)(aq)
	12.6	FA1-Cu(6)(aq)
HFA2-(6)(aq)	20.0	HFA2-(6)(aq)
	16.5	FA2-Cu(6)(aq)
	63.4	FA2-H(6)(aq)
MOPS-1	69.7	MOPS-1
	30.3	H-MOPS (aq)

Solids data

Mineral	Saturation index (= log IAP – log Ks)	Minerals precipitated	Equilibrium amount (mol L^{-1})
Atacamite	0	Atacamite	2.02E-05
$Cu(OH)_2(s)$	-0.821		

c) 50 µmol L^{-1} Cu (II), 0 µmol L^{-1} S(-II), 50 mg C L^{-1} SRFA

Input

Species	Na^+ (mol L^{-1})	Cl^- (mol L^{-1})	MOPS (mol L^{-1})	SRFA (mg C L^{-1})	Cu(II) (µmol L^{-1})	pH
Concentration	0.01	0.01	0.001	50	50	7.5

Distribution of components between dissolved and precipitated species (in mol L^{-1})

Component	Total dissolved	% dissolved	Dissolved inorganic	Bound to DOM	% bound to DOM	Total precipitated	% precipitated
Cu(II)	5.00E-05	100	9.90E-08	4.99E-05	99.8	0	0
Cl^-	1.00E-02	100	1.00E-02	0	0	0	0

Dissolved data

Component	% of total concentration	Species
Cu^{2+}	0.1	Cu+2
	29.2	FA2-Cu(6)(aq)
	0.1	CuOH+
	0.5	(6)Cu+2D(aq)
	70.1	FA1-Cu(6)(aq)
HFA1-(6)(aq)	89.7	HFA1-(6)(aq)
	3.1	FA1-H(6)(aq)
	7.2	FA1-Cu(6)(aq)
HFA2-(6)(aq)	12.4	HFA2-(6)(aq)
	9.5	FA2-Cu(6)(aq)
	78.1	FA2-H(6)(aq)
MOPS-1	69.7	MOPS-1
	30.3	H-MOPS (aq)

Solids data

Mineral	Saturation index (= log IAP – log Ks)	Minerals precipitated	Equilibrium amount (mol L^{-1})
Atacamite	-1.813	none	-
$Cu(OH)_2(s)$	-1.728		

d) 500 µmol L^{-1} Cu (II), 0 µmol L^{-1} S(-II), 0 mg C L^{-1} SRFA

Input

Species	Na^+ (mol L^{-1})	Cl^- (mol L^{-1})	MOPS (mol L^{-1})	SRFA (mg C L^{-1})	Cu(II) (µmol L^{-1})	pH
Concentration	0.01	0.01	0.01	0	500	7.5

Distribution of components between dissolved and precipitated species (in mol L^{-1})

Component	Total dissolved	% dissolved	Total precipitated	% precipitated
Cu(II)	8.16E-07	0.16	4.99E-04	99.84
Cl^-	9.75E-03	97.50	2.50E-04	2.50

Solids data

Mineral	Saturation index (= log IAP – log Ks)	Minerals precipitated	Equilibrium amount (mol L^{-1})
Atacamite	0	Atacamite	2.50E-04
$Cu(OH)_2(s)$	-0.816		

e) 500 µmol L^{-1} Cu (II), 0 µmol L^{-1} S(-II), 50 mg C L^{-1} SRFA

Input

Species	Na^+ (mol L^{-1})	Cl^- (mol L^{-1})	MOPS (mol L^{-1})	SRFA (mg C L^{-1})	Cu(II) (µmol L^{-1})	pH
Concentration	0.01	0.01	0.01	50	500	7.5

Distribution of components between dissolved and precipitated species (in mol L^{-1})

Component	Total dissolved	% dissolved	Dissolved inorganic	Bound to DOM	% bound to DOM	Total precipitated	% precipitated
Cu(II)	9.00E-05	18.00	8.14E-07	8.92E-05	99.1	4.10E-04	82.00
Cl^-	9.79E-03	97.95	9.79E-03	0	0.0	2.05E-04	2.05

Dissolved data

Component	% of total concentration	Species
Cu^{2+}	0.5	Cu+2
	28.2	FA2-Cu(6)(aq)
	0.4	CuOH+
	0.0	Cu(OH)2 (aq)
	1.6	(6)Cu+2D(aq)
HFA1-(6)(aq)	69.3	FA1-Cu(6)(aq)
	85.3	HFA1-(6)(aq)
	1.9	FA1-H(6)(aq)
HFA2-(6)(aq)	12.8	FA1-Cu(6)(aq)
	20.0	HFA2-(6)(aq)
	16.5	FA2-Cu(6)(aq)
MOPS-1	63.4	FA2-H(6)(aq)
	69.7	MOPS-1

Solids data

Mineral	Saturation index (= log IAP – log Ks)	Minerals precipitated	Equilibrium amount (mol L^{-1})
Atacamite	0	Atacamite	2.05E-04
$Cu(OH)_2(s)$	-0.817		

Table S7: Speciation of final Cu_xS suspensions (after sulfide addition) as calculated with Visual MINTEQ 3.1. Suspensions with different SRFA concentrations and absolute concentrations are presented (a-e).

a) 50 µmol L^{-1} Cu (II), 100 µmol L^{-1} S(-II), 0 mg C L^{-1} SRFA

Input

Species	Na^+ (mol L^{-1})	Cl^- (mol L^{-1})	MOPS (mol L^{-1})	SRFA (mg C L^{-1})	Cu(II) (µmol L^{-1})	S(-II) (µmol L^{-1})	pH
Concentration	0.01	0.01	0.001	0	50	100	7.5

Distribution of components between dissolved and precipitated species (in mol L^{-1})

Component	Total dissolved	% dissolved	Total precipitated	% precipitated
Cu(II)	0	0	5.00E-05	100.00
HS^-	7.84E-07	0.784	9.92E-05	99.22

Solids data

Mineral	Saturation index (= log IAP – log Ks)	Minerals precipitated	Equilibrium amount (mol L^{-1})
Covellite	0	Covellite	5.00E-05
Sulfur(s)	0	Sulfur(s)	4.92E-05
Atacamite	-33.850		
$Cu(OH)_2(s)$	-17.746		

b) 50 µmol L^{-1} Cu (II), 100 µmol L^{-1} S(-II), 5 mg C L^{-1} SRFA

Input

Species	Na^+ (mol L^{-1})	Cl^- (mol L^{-1})	MOPS (mol L^{-1})	SRFA (mg C L^{-1})	Cu(II) (µmol L^{-1})	S(-II) (µmol L^{-1})	pH
Concentration	0.01	0.01	0.001	5	50	100	7.5

Distribution of components between dissolved and precipitated species (in mol L^{-1})

Component	Total dissolved	% dissolved	Total precipitated	% precipitated
Cu(II)	0	0	5.00E-05	100.00
HS^-	7.84E-07	0.784	9.92E-05	99.22

Solids data

Mineral	Saturation index (= log IAP – log Ks)	Minerals precipitated	Equilibrium amount (mol L^{-1})
Covellite	0	Covellite	5.00E-05
Sulfur(s)	0	Sulfur(s)	4.92E-05
Atacamite	-33.850		
$Cu(OH)_2(s)$	-17.746		

c) 50 µmol L^{-1} Cu (II), 100 µmol L^{-1} S(-II), 50 mg C L^{-1} SRFA

Input

Species	Na^+ (mol L^{-1})	Cl^- (mol L^{-1})	MOPS (mol L^{-1})	SRFA (mg C L^{-1})	Cu(II) (µmol L^{-1})	S(-II) (µmol L^{-1})	pH
Concentration	0.01	0.01	0.001	50	50	100	7.5

Distribution of components between dissolved and precipitated species (in mol L^{-1})

Component	Total dissolved	% dissolved	Total precipitated	% precipitated
Cu(II)	0	0	5.00E-05	100.00
HS^-	7.84E-07	0.784	9.92E-05	99.22

Solids data

Mineral	Saturation index (= log IAP – log Ks)	Minerals precipitated	Equilibrium amount (mol L^{-1})
Covellite	0	Covellite	5.00E-05
Sulfur(s)	0	Sulfur(s)	4.92E-05
Atacamite	-33.850		
$Cu(OH)_2(s)$	-17.746		

d) 500 µmol L^{-1} Cu (II), 1000 µmol L^{-1} S(-II), 0 mg C L^{-1} SRFA

Input

Species	Na^+ (mol L^{-1})	Cl^- (mol L^{-1})	MOPS (mol L^{-1})	SRFA (mg C L^{-1})	Cu(II) (µmol L^{-1})	S(-II) (µmol L^{-1})	pH
Concentration	0.01	0.01	0.01	0	500	1000	7.5

Distribution of components between dissolved and precipitated species (in mol L^{-1})

Component	Total dissolved	% dissolved	Total precipitated	% precipitated
Cu(II)	0	0	5.00E-05	100.00
HS^-	7.84E-07	0.784	9.92E-05	99.22

Solids data

Mineral	Saturation index (= log IAP – log Ks)	Minerals precipitated	Equilibrium amount (mol L^{-1})
Covellite	0	Covellite	5.00E-04
Sulfur(s)	0	Sulfur(s)	4.99E-04
Atacamite	-33.850		
$Cu(OH)_2(s)$	-17.746		

e) 500 µmol L^{-1} Cu (II), 1000 µmol L^{-1} S(-II), 50 mg C L^{-1} SRFA

Input

Species	Na^+ (mol L^{-1})	Cl^- (mol L^{-1})	MOPS (mol L^{-1})	SRFA (mg C L^{-1})	Cu(II) (µmol L^{-1})	S(-II) (µmol L^{-1})	pH
Concentration	0.01	0.01	0.01	50	500	1000	7.5

Distribution of components between dissolved and precipitated species (in mol L^{-1})

Component	Total dissolved	% dissolved	Total precipitated	% precipitated
Cu(II)	0	0	5.00E-05	100.00
HS^-	7.84E-07	0.784	9.92E-05	99.22

Solids data

Mineral	Saturation index (= log IAP – log Ks)	Minerals precipitated	Equilibrium amount (mol L^{-1})
Covellite	0	Covellite	5.00E-04
Sulfur(s)	0	Sulfur(s)	4.99E-04
Atacamite	-33.850		
$Cu(OH)_2(s)$	-17.746		

Testing for significant differences in the TEM-derived central tendency and particle size distributions among the Cu_xS suspensions

In order to test for significant differences among median minimum Feret TEM diameters and number-based TEM particle size distributions of the dilute as well as concentrated Cu_xS suspensions of the growth experiment, we applied a pairwise Wilcoxon-Mann-Whitney U-test (Table S8 – S10). As input, TEM-derived minimum Feret diameters of all particles from a suspension were used and compared with the ones from another suspension (comparisons as seen in the Tables S8 – S10 below) in a pairwise manner. Significant differences were tested at different α-levels.

Table S8: Tests for significant differences among median TEM diameters and PSDs of the dilute Cu_xS suspensions of the growth experiment.

Wilcoxon-Mann-Whitney U-test for testing differences in the central tendency (median particle size) and the particle size distribution of samples Green: significant difference at given α-level Red: no significant difference at given α-level	**Dilute suspensions** (50 µmol L^{-1} Cu(II), 100 µmol L^{-1} S(-II))	**0 mg C L^{-1} SRFA**				**5 mg C L^{-1} SRFA**				**50 mg C L^{-1} SRFA**			
Dilute suspensions (50 µmol L^{-1} Cu(II), 100 µmol L^{-1} S(-II))		100 min	24 h	7 d	28 d	100 min	24 h	7 d	28 d	100 min	24 h	7 d	28 d
0 mg C L^{-1} SRFA	100 min		0.001	0.001	0.001	0.001				0.001			
	24 h			0.001	0.001		0.001				0.001		
	7 d				0.001			0.001				0.001	
	28d								0.001				0.001
5 mg C L^{-1} SRFA	100 min						0.001	0.001	0.001	0.001			
	24 h							0.001	0.001		0.001		
	7 d								0.001			0.001	
	28d												0.05
50 mg C L^{-1} SRFA	100 min										0.001	0.001	0.001
	24 h											0.001	0.001
	7 d												0.001
	28d												

Table S9: Tests for significant differences among median TEM diameters and PSDs of the concentrated Cu_xS suspensions of the growth experiment (I).

Wilcoxon-Mann-Whitney U-test for testing differences in the central tendency (median particle size) and the particle size distribution of samples Green: significant difference at given α-level Red: no significant difference at given α-level	**Dilute suspensions** (50 µmol L^{-1} Cu(II), 100 µmol L^{-1} S(-II))	**0 mg C L^{-1} SRFA**				**5 mg C L^{-1} SRFA**				**50 mg C L^{-1} SRFA**			
Concentrated suspensions (500 µmol L^{-1} Cu(II), 1000 µmol L^{-1} S(-II))		100 min	24 h	7 d	28 d	100 min	24 h	7 d	28 d	100 min	24 h	7 d	28 d
0 mg C L^{-1} SRFA	100 min	0.001											
	24 h		0.001										
	7 d			0.001									
	28d				0.001								
50 mg C L^{-1} SRFA	100 min					0.001				0.001			
	24 h						0.001				0.001		
	7 d							0.001				0.001	
	28d								0.001				0.001

Table S10: Tests for significant differences among median TEM diameters and PSDs of the concentrated Cu_xS suspensions of the growth experiment (II).

Wilcoxon-Mann-Whitney U-test for testing differences in the central tendency (median particle size) and the particle size distribution of samples Green: significant difference at given α-level Red: no significant difference at given α-level	**Concentrated suspensions** (500 µmol L^{-1} Cu(II), 1000 µmol L^{-1} S(-II))	**0 mg C L^{-1} SRFA**				**50 mg C L^{-1} SRFA**			
Concentrated suspensions (500 µmol L^{-1} Cu(II), 1000 µmol L^{-1} S(-II))		100 min	24 h	7 d	28 d	100 min	24 h	7 d	28 d
0 mg C L^{-1} SRFA	100 min		0.001	0.001	0.001	0.001			
	24 h			0.1	0.1		0.1		
	7 d				0.1			0.001	
	28d								0.05
50 mg C L^{-1} SRFA	100 min						0.001	0.001	0.001
	24 h							0.1	0.05
	7 d								0.001
	28d								

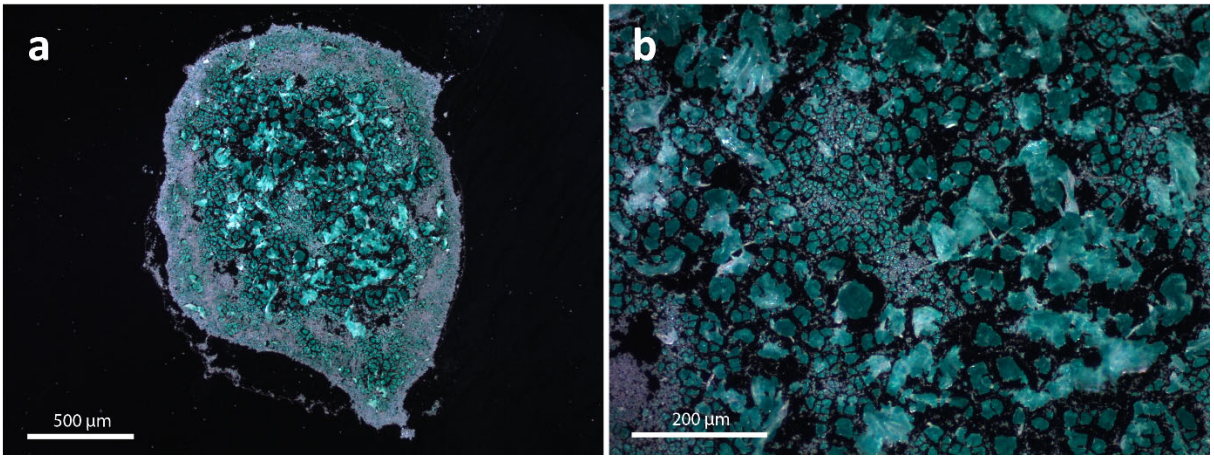

Figure S20: Light microscope images of the Cu precipitate isolated from a 30 min old precursor solution. For isolation of the Cu precipitate, 15 mL of a (30 min old) concentrated (500 µmol L^{-1} Cu) SRFA-free precursor solution (no sulfide) was ultrafiltrated (Amicon Ultra 3 kDa ultrafiltration membrane) at 20°C for 15 min at 3500 rpm. Precipitates retained to the filter membranes were resuspended in ultrapure water with a pipette, recovered and transferred into an Eppendorf tube. Then, this suspension was centrifuged at room temperature for 15 min at 15000 rpm. The supernatant was removed and the obtained solid was reconstituted in 100 µL ethanol. This ethanolic suspension was then repetitively deposited and dried onto a zero background silicon wafer (orientation (510), Siltronix, France) until a thin precipitate layer was visible. The Cu-phase could not be determined with XRD. However, the observed color strongly resembles colors typical for Cu hydroxide or (par)atacamite phases.

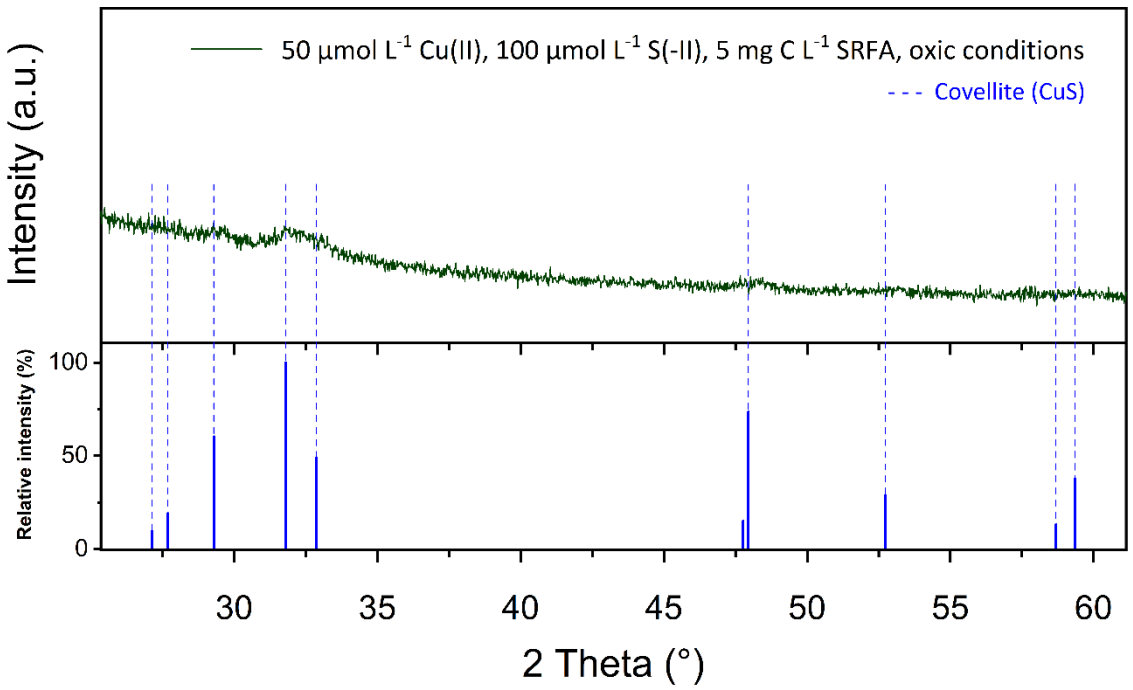

Figure S21: X-ray diffractogram of a the remaining solid fraction of a Cu_xS suspension from the oxidative dissolution experiment exposed to dissolved dioxygen for over 100 d. After this period of time, only covellite and no Cu hydroxides were found. The bottom part of the figure shows the major reflections (with their relative intensities) of covellite. Dashed lines originating from these reflections show the (qualitative) peak matching analysis with the recorded diffractograms.

Composition: 50 µmol L^{-1} Cu(II), 100 µmol L^{-1} S(-II), 0 mg C L^{-1} SRFA, pH 7.5, IS: 10 mmol L^{-1} NaCl

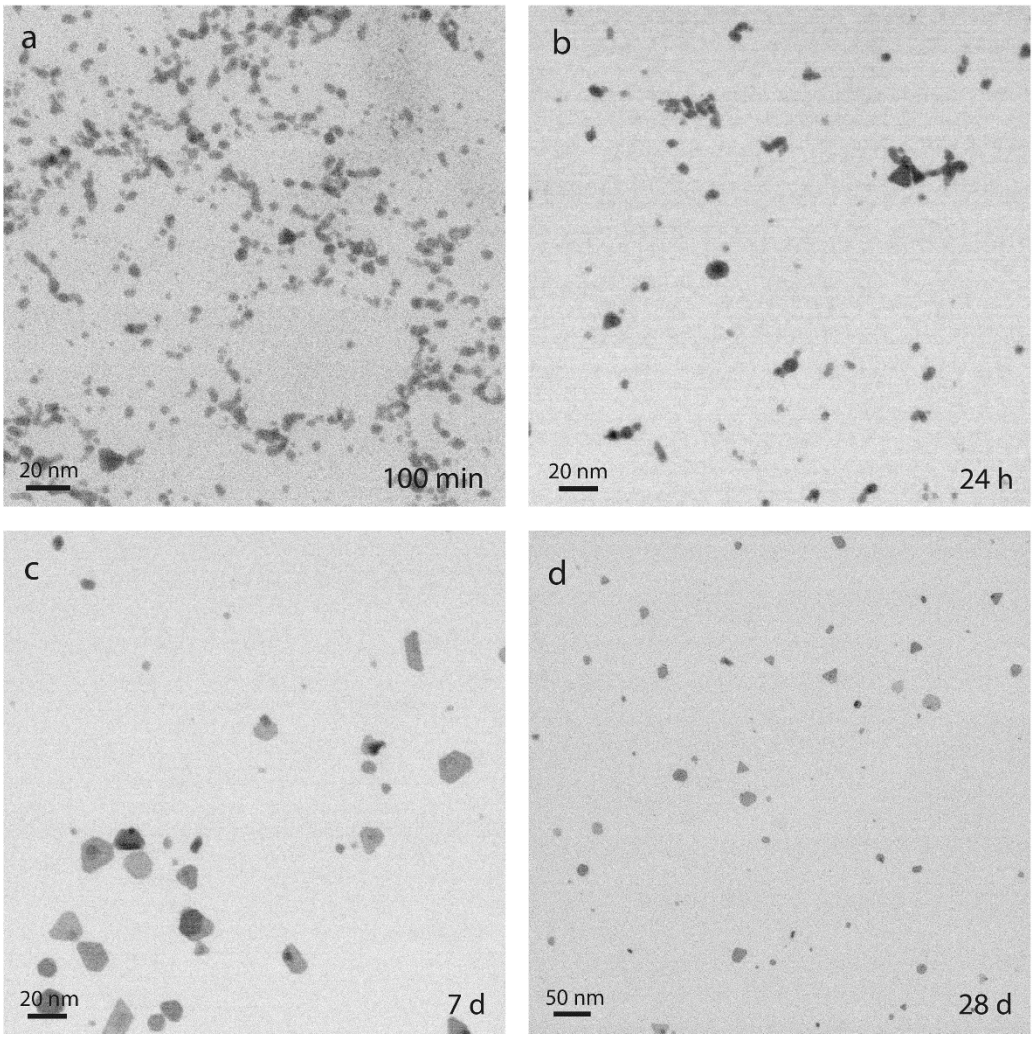

Figure S22: HAADF-TEM images (shown as inverted images) of dilute, SRFA-free Cu_xS suspensions at different times of the growth experiment.

References

1. Smoluchowski, M., Elektrische Endosmose und Strömungsströme, *Pisma Mariana Smoluchowskiego*, 1928, **3**, 246-346.
2. Gustafsson, J. P., Visual MINTEQ ver. 3.1, 2013, https://vminteq.lwr.kth.se/, (accessed 25.11.2019).
3. Milne, C. J., Kinniburgh, D. G., van Riemsdijk, W. H. and Tipping, E., Generic NICA−Donnan Model Parameters for Metal-Ion Binding by Humic Substances, *Environmental Science & Technology*, 2003, **37**, 958-971.